



Article

Spatial Influence of Multifaceted Environmental States on Habitat Quality: A Case Study of the Three Largest Chinese Urban Agglomerations

Fei Liu ^{1,*}, Yuji Murayama ² and Yoshifumi Masago ¹

¹ Center for Climate Change Adaptation, National Institute for Environmental Studies, 16-2 Onogawa, Tsukuba 305-8506, Ibaraki, Japan

² Faculty of Life and Environmental Sciences, University of Tsukuba, Tsukuba 305-8572, Ibaraki, Japan

* Correspondence: liu.fe@nies.go.jp; Tel.: +81-29-850-2387

Abstract: Habitat structure and quality in the urban agglomeration (UA) are subject to multiple threats and pressures due to ongoing anthropogenic activities and call for comprehensively effective solutions. Many approaches, including cartographic comparison, correlation analysis, the local entropy model, and GeoDetector, were jointly used to clarify the interplay between habitat quality and multiple environmental issues. In response to the overlapped risks of diverse environmental systems, this study presented an integrated research framework to evaluate the spatial influences of multifaceted environmental situations on habitat quality. We conducted the case study in the three largest Chinese UAs: Beijing–Tianjin–Hebei (BTH), Greater Bay Area (GBA), and Yangtze River Delta (YRD). The evaluation results show that the three UAs shared similarities and differences in relationship/impact types and their strengths. In 2015, most of the three UAs' landscapes delivered low–medium magnitudes of habitat quality (score <0.7) and emerged with unevenly severe consequences over space across different environmental aspects, highlighting the importance of maintaining habitat safety. Overall, habitat quality scores were synergistic with NDVI, but antagonistic to surface heat island intensity (SHII), PM2.5 concentrations, and residential support. However, locally structured relationships exhibited geographical complexity and heterogeneity between habitat quality and environmental systems. Regarding GeoDetector evaluation, PM2.5 concentrations in BTH, SHII in GBA, and NDVI in YRD played a dominant role in single-factor and interaction analysis. More importantly, the synergistic effect of various environmental issues on habitats was manifested as mutually enhanced rather than independent or weakened interactive effects, implying the aggravation of compound effects and the necessity of prioritization schemes. This study could provide beneficial insights into the interconnections between habitats' sustainability and multifaceted environmental situations in UAs.

Keywords: air quality; GeoDetector; habitat quality; thermal environment; urban agglomeration



Citation: Liu, F.; Murayama, Y.; Masago, Y. Spatial Influence of Multifaceted Environmental States on Habitat Quality: A Case Study of the Three Largest Chinese Urban Agglomerations. *Remote Sens.* **2023**, *15*, 921. <https://doi.org/10.3390/rs15040921>

Academic Editor: Riccardo Buccolieri

Received: 4 December 2022

Revised: 3 February 2023

Accepted: 4 February 2023

Published: 7 February 2023



Copyright: © 2023 by the authors. Licensee MDPI, Basel, Switzerland. This article is an open access article distributed under the terms and conditions of the Creative Commons Attribution (CC BY) license (<https://creativecommons.org/licenses/by/4.0/>).

1. Introduction

Ongoing socioeconomic development has given rise to multifaceted problems and challenges for habitats. The Intergovernmental Panel on Climate Change (IPCC) highlighted the necessity of understanding the interrelationships and linkages between various environmental issues in the Sixth Assessment Report [1]. The natural ecosystem and human system are intertwined, and alterations in one component may stimulate others [1]. Thus, sustainable development strategies require a new understanding of compound environmental issues and overlapping consequences [2].

The United Nations declared that over half of the current world's dwellers reside in urban settlements in the World Urbanization Prospects [3]. This proportion will rise to two-thirds by the 2050s [3]. Accordingly, improving human well-being increasingly relies on upgrading the situations and services in human-dominated urban areas [4,5].

Urban agglomerations (UAs) are a newly evolved manifestation of spatially clustered regions with a common interest and fate [6]. Regional integration development and drastic urbanization have propelled the formation of UAs [7]. The UA system is a complex ensemble comprising multiple cities and their extended outskirts with large-scale urban fabrics and artificial landscapes. These artificial landscapes provide adequate space to guarantee social-economic boom and human well-being [6]. In parallel, natural habitats provide a majority of essential ecosystem services to sustain the ecological security of the entire UA region. However, with drastic economic and population growth, UA regions have manifested vigorous trade-offs between ecosystem services provision and human social development, giving rise to enormous ecological deficits, especially in the core megacities and highly populated areas [4,8]. As such, the habitats of UAs are diverse but fragile, and might be subjected to a multitude of risk factors from natural and human interference [4].

Existing studies on UAs are typically confined to the individual environmental problem, formation mechanism, and mitigation strategy, including the thermal [9], air [10], housing [11], landscape [12], and resource [13] spheres. A vast quantity of studies have identified, for example, the heat island phenomenon [14,15], air pollution [16,17], and urban containment [18]. Abundant solutions have continuously contributed to a future sustainable world, such as nature-based solutions [19] and ecological intensification interventions [20]. Against the backdrops of UAs, implementing measures that safeguard environmental health and human well-being across multiple aspects is warranted [21,22]. However, few studies have been concerned with the fate of compound environmental risks and their interactive relationships. The environmental crisis in the UAs may be magnified due to the overlap of multiple issues, their influences on habitats may be aggravated, and comprehensive carrying capacity might have further deteriorated [1,23]. Considering the growing demands for comprehensive issues and compound risks in the UAs, it is imperative to understand the associations between diffident environmental problems and seek co-benefits.

Unraveling the relationships between habitats and environmental issues is the foundation of effective, comprehensive policies. Yet, one of the key challenges is obtaining insights into the complex interplay of multiple environmental situations [1,4]. The impact of human interference on different environment systems varies broadly from slight, modest, to severe, but may share similar driving factors [8,24–26]. Additionally, the measurement of the geographical association of multiple variables relies on their locations, distances, neighboring settings, and scales [24,27,28]. However, conventional methods, such as cartographic comparison, correlation, and regression analysis, generally only mirror simple relationships [29]. Exponential, quadratic, and interactive relationships are difficult to represent using these conventional methods. The lack of knowledge about complex relationships has obstructed the achievement of multifaceted environmental evaluation [29]. In light of this, this study presents a framework that integrates multi-method and multi-source data to evaluate the associations between multifaceted environmental states and habitat quality in different UA settings. Our proposed framework incorporates cartographic comparison, correlation analysis, the local entropy model, and GeoDetector to conduct a spatially multi-perspective relationship profiling. The local entropy model is a novel method for examining the locally varying relationships over space, which can capture linear and polynomial complex associations [29]. GeoDetector is a powerful tool for identifying spatial stratified heterogeneities and interactive effects [30,31].

We designated the UAs of Beijing–Tianjin–Hebei (BTH), Guangdong–Hong Kong–Macao Greater Bay Area (GBA), and Yangtze River Delta (YRD) as the study regions. In recent decades, the Chinese government has been committed to ecological civilization construction and sustainability management in these three UAs based on a series of relevant initiatives and policies [32–34], which have been in response to habitat degradation from dramatic socioeconomic growth [13,35–38]. Moreover, many scientific investigations have contributed to sustainable development schemes for the three UAs [37,39–44]. The thermal environment, air quality, living space, and green landscapes have been the focal topics

among environmental monitoring and assessments, which are also deeply discussed in this study. Thus, focusing on the three UAs of BTH, GBA, and YRD in 2015, this study consists of four goals, as follows: (1) Quantification of habitat quality; (2) Evaluation of diverse environmental situations from the thermal, air, living, and landscape spheres; (3) Identification of the interconnection and interplay between habitat quality and multi-dimensional environmental situations; and (4) Elucidation of a potential management pathway for multi-dimensional sustainability and security for the UAs.

2. Materials and Methods

2.1. Study Areas

This study focused on the three largest Chinese UAs: BTH, GBA, and YRD (Figure 1). The study regions were determined due to (1) their rapid socioeconomic development, (2) plentiful nature capitals, (3) critical geographical location, (4) urgent sustainability needs, and (5) superior policy support. BTH, GBA, and YRD are nationally and globally representative UA regions. These UA regions are not only primary engines and important pivots for China's socioeconomic development, but also the significant guarantee and forefront of China's ecological security. BTH UA ($113^{\circ}27'E$ to $119^{\circ}50'E$, $35^{\circ}03'N$ to $42^{\circ}40'N$) is situated in Northeast China, encompassing 13 cities with 2.2% (2.2×10^7 ha) of the national territorial area. GBA UA ($111^{\circ}27'E$ to $115^{\circ}42'E$, $21^{\circ}57'N$ to $24^{\circ}40'N$) has a scope of 9 cities and 2 special administrative regions in South China, accounting for 0.6% (5.6×10^6 ha) of the national territory. YRD UA ($111^{\circ}27'E$ to $115^{\circ}42'E$, $21^{\circ}57'N$ to $24^{\circ}40'N$) is composed of 16 cities on the eastern coast of China, covering 2.2% of China's territory (2.1×10^7 ha).

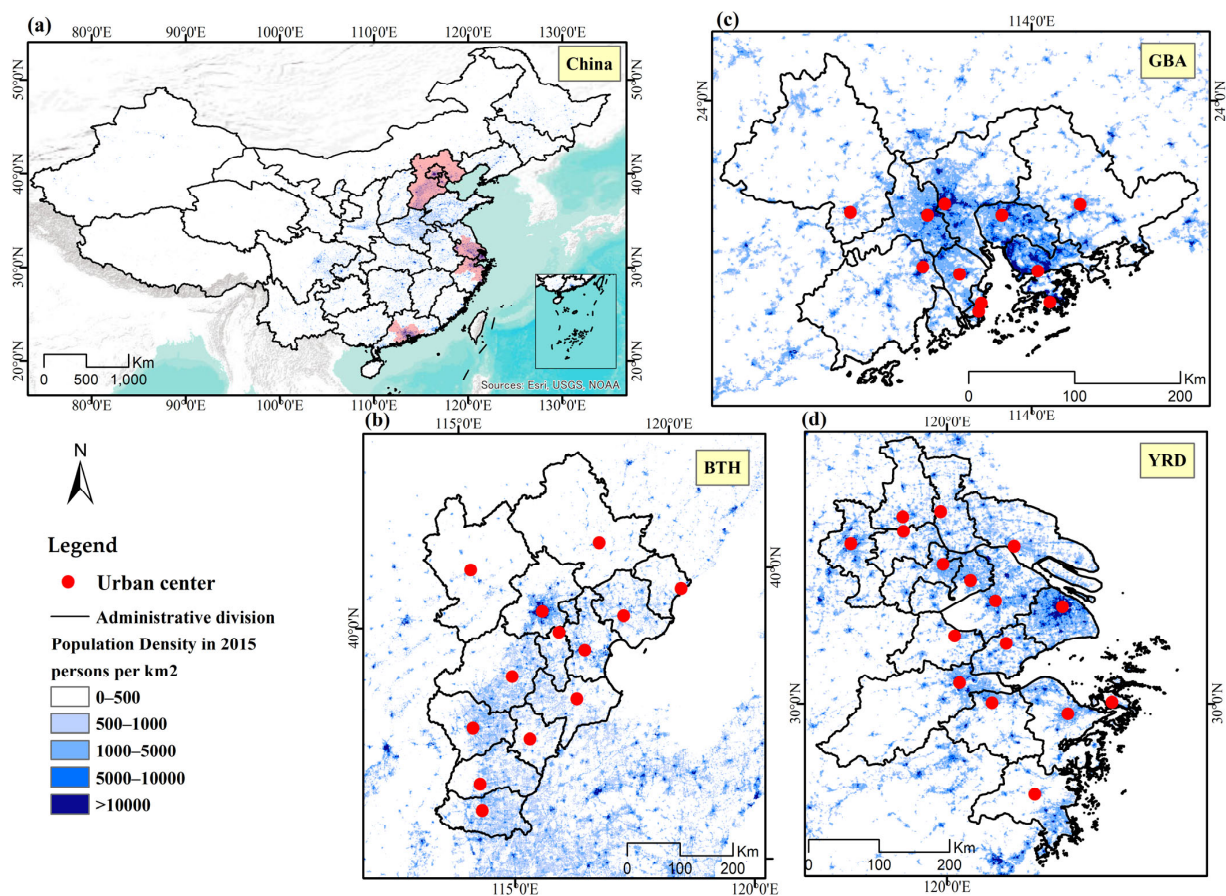


Figure 1. Study areas: (a) geographic location of the study areas in China; (b) Beijing–Tianjin–Hebei (BTH); (c) Guangdong–Hong Kong–Macao Greater Bay Area (GBA); and (d) Yangtze River Delta (YRD).

At the end of 2015, approximately 8%, 5%, and 11% of the national population resided in BTH, GBA, and YRD, respectively [45]. BTH, GBA, and YRD had 10.2%, 14%, and 18.5% of the

respective national totals in the gross domestic product (GDP) [45]. These three UAs emerge as compound habitat systems of multiple urban cores and their peripheral countrysides under different climate schemes characterized by abundant land details. BTH, GBA, and YRD are configured by a variety of ecosystems, landscapes, and landforms. BTH is located in a temperate monsoon climate zone, while GBA and YRD are dominated by a monsoon subtropical climate context. Significant alterations and transformations in the environmental landscapes and socioeconomic scales of these UAs in recent decades [38,42,46,47] have given rise to habitat degradation, ecological fragility, and climate crisis [48–51], such as intensified heat island effects [52] and deteriorated air pollution [16]. Thus, national development initiatives also highlight the urgency and necessity of sustainability-related, ecological-oriented strategies and projects in BTH, GBA, and YRD [32–34].

2.2. Data Preparation and Treatment

Given the data availability, precision, and consistency of the three UAs, this study set 2015 as the year for the research. The year 2015 was an extraordinary time for economic growth and social boom in BTH, GBA, YRD, and even the entire territory of China due to a number of important development policies, including the 13th Five-Year Plan, Belt and Road initiatives, and regional collaboration plans [32–34,53].

The land cover/use maps of the BTH, GBA, and YRD in 2015 were cited and pruned from Climate Change Initiative (CCI) global land cover (LC) products, European Space Agency (ESA) (<https://www.esa-landcover-cci.org/> (accessed on 30 November 2022)). ESA CCI-LC product is a 300 m spatial resolution of a time-series global surface coverage dataset generated based on multi-source satellite archives [54]. The overall weighted-area accuracy of the ESA CCI-LC map in 2015 was validated to be 71.1% [54]. Thus, the ESA CCI-LC map can deliver abundant land details and flexibly serve diverse land-oriented applications. Referring to the official classification scheme [54] and IUCN habitat-related suggestions [55,56], we rearranged the land cover/use thematic legend into eight categories: agricultural habitat (AH), forest habitat (FH), grassland habitat (GH), wetland habitat (WH), shrubland habitat (SH), urban fabric (UF), vacant land (VL), and water (WA).

The annual average daytime and nighttime land surface temperatures (LSTs) of the BTH, GBA, and YRD in 2015 were composited and preprocessed based on the 1 km resolution of Moderate Resolution Imaging Spectroradiometer (MODIS) daily/night land surface temperature/emissivity products (MOD11A1 and MYD11A1, <https://modis.gsfc.nasa.gov/data/dataproduct/mod11.php> (accessed on 30 November 2022)) using the Google Earth Engine (GEE). The 2015 yearly average normalized difference vegetation index (NDVI) distributions in the BTH, GBA, and YRD were also GEE-derived and composed using MODIS 1 km 16-Day vegetation indices (MOD13A2, <https://modis.gsfc.nasa.gov/data/dataproduct/mod13.php> (accessed on 30 November 2022)). The 1 km resolution spatial coverages of the 2015 average PM_{2.5} (particulate matter in the air with aerodynamic diameters smaller than 2.5 µm) concentrations in the BTH, GBA, and YRD were sourced from China High Air Pollutants (CHAP) datasets [57,58] (<https://weijing-rs.github.io/product.html> (accessed on 30 November 2022)). The China High PM_{2.5} datasets were developed by coupling in site PM_{2.5} data, MODIS aerosol optical depth (AOD) products, and various auxiliary data based on the space-time extra-trees model [57]. Various air-relevant studies have used the ChinaHighPM_{2.5} datasets due to their wide spatiotemporal range and high cross-validation accuracy ($R^2 = 0.86–0.90$) [57,58]. Spatially gridded population density data (1 km of spatial resolution) of the BTH, GBA, and YRD in 2015 were extracted from the high-profile WorldPop population products. WorldPop (<https://www.worldpop.org/> (accessed on 30 November 2022)), developed by the University of Southampton, has been dedicated to supporting the open utilization of various spatial demographic studies [59]. China-relevant spatial data (e.g., administrative boundary) were obtained from the Resource and Environmental Science and Data Center, Chinese Academy of Sciences (<https://www.resdc.cn/Default.aspx> (accessed on 30 November 2022)).

2.3. Research Framework

This study aims to evaluate the interconnection and spatial heterogeneity between habitat quality and multiple environmental situations from multiple perspectives. Thus, the cascade diagram of our proposed framework is shown in Figure 2. The overall research framework is mainly composed of four modules: (I) data preparation and preprocessing; (II) correlation analysis; (III) local bivariate analysis; and (IV) GeoDetector analysis.

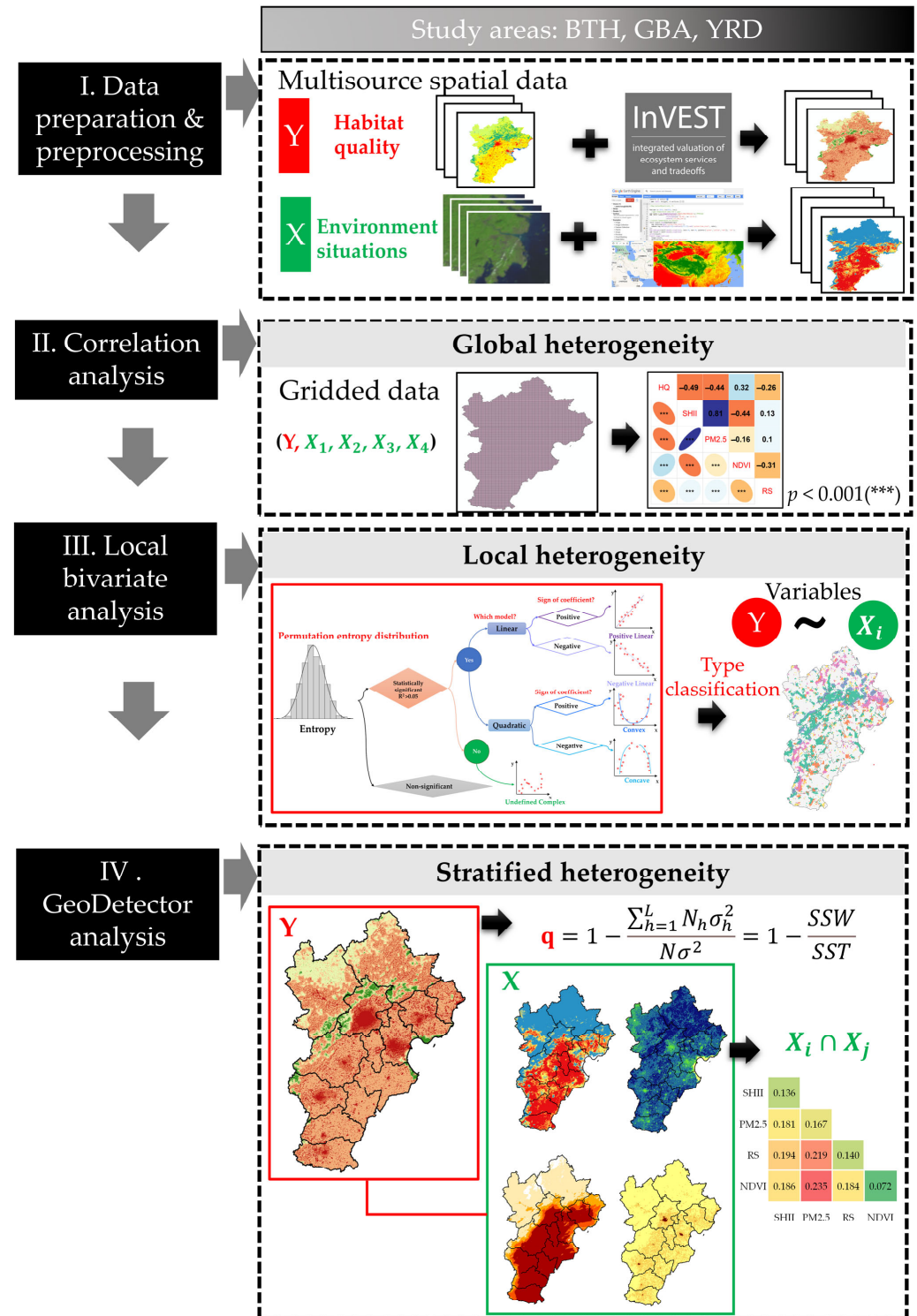


Figure 2. Overall research framework. Note: InVEST logo image sources from the website (<https://naturalcapitalproject.stanford.edu/software/invest> (accessed on 30 November 2022)).

2.4. Quantification of Habitat Quality

Habitat quality is geographically heterogeneous, which depends on habitat characteristics, suitability, and the presence and relative magnitudes of threat factors [60]. In light of this, the spatial patterns and magnitudes could be evaluated by the joint use of land cover/use and threats data [61,62]. The Integrated Valuation of Ecosystem Services and Tradeoffs–Habitat Quality (InVEST–HQ) model was developed by Natural Capital Projects in conjunction with Stanford University, the Nature Conservancy, and the World Wide Fund for Nature (<https://naturalcapitalproject.stanford.edu/software/invest> (accessed on 30 November 2022)). Given the low data demand, superior spatial visualization, and easy operation, the InVEST–HQ model is the dominant tool for habitat quality quantification. It has been widely applied to ecological studies across different regions and spatial scales [60]. Thus, we employed the InVEST–HQ model to estimate the habitat quality in the three UAs of BTH, GBA, and YRD. Habitat quality can be calculated using the following equations:

$$Q_{xj} = H_j \left(1 - \left(\frac{D_{xj}^z}{D_{xj}^z + k^z} \right) \right) \quad (1)$$

where Q_{xj} represents the habitat quality of grid x in land cover/use type j ; H_j refers to the habitat suitability of land cover/use type j ; D_{xj} reflects the total threat level in grid cell x with land cover/use type j , which is judged by the types, intensities, and proximities of neighboring threats [62]; k is the half-saturation constant, which is equivalent to the half of the crest value of D_{xj} ; and z is default at 2.5, which is a scaling parameter for mirroring spatial differentiation [60].

$$D_{xj} = \sum_{r=1}^R \sum_{y=1}^{Y_r} \left(\frac{w_r}{\sum_{r=1}^R w_r} \right) r_y i_{rxy} \beta_x S_{jr} \quad (2)$$

where R denotes the number of threats; y indexes all grid cells on the raster layer of threat r ; Y_r indicates the set of grid cells occupied by the threat on the raster layer; w_r and r_y reflect the weight of the threat and the interference intensity of the threat for grid cell y , respectively; i_{rxy} is the habitat interference level of grid cell x from threat r on the grid cell y ; β_x refers to the reachability level (the anti-disturbance ability) of grid cell x ; and S_{jr} represents the relative sensitivity of land cover/use type j to threat factor r . The habitat quality scores range from 0 to 1, which embodies serious to ideal situations for habitat quality [60]. In this paper, i_{rxy} was considered as follows:

$$i_{rxy} = 1 - \left(\frac{d_{xy}}{d_{r \max}} \right) \text{ if linear attenuation} \quad (3)$$

$$i_{rxy} = \exp \left(- \left(\frac{2.99}{d_{r \max}} \right) d_{xy} \right) \text{ if exponential decay} \quad (4)$$

where d_{xy} is the linear distance between grid cells x and y , and $d_{r \max}$ is the maximum effective influence distance of threat r . More specific information is provided in the InVEST user guide [60] and the relevant literature [35,49,63–66].

We primarily prepared three categories of documentation as input parameters of the InVEST–HQ model: (1) raster layers of land cover/use, (2) threat data, sources, and their accessibility, and (3) suitable habitat types and corresponding threat sensitivities [60]. Threat sources in this study included cultivated lands, bare lands, and built-up lands due to data availability and consistency. The raster layers of threat sources were derived in ArcGIS Pro Version 3.0.1 (<https://www.esri.com/products/arcgis-pro/> (accessed on 30 November 2022)). The setting of threat factors and sensitivity parameters were based on previous literature in the study regions, expert knowledge, and the official user guide manual [35,49,60,63–66], as shown in the Supplementary Materials.

2.5. Evaluation of Multifaceted Environmental States

Land surface temperature (LST) is an essential key variable in surface energy balance, heat fluxes, and energy exchanges over different land cover types, playing a crucial role in geo-environmental and human health [28]. Thermal infrared (TIR) data from satellite platforms and retrieved LST are reliable barometers for diagnosing thermal circumstances in various fields [28,67]. Numerous studies have found different responses to daytime and nighttime LSTs and reported their different influences on environmental situations and human behaviors [28,67]. Thus, we utilized both daytime and nighttime LSTs. Instead of absolute LST observations, the intensity of the surface heat island (SHII) was estimated for evaluating the states of thermal environments in BTH, GBA, and YRD to minimize the effects and uncertainty of the climate background. The SHII was generated using the average daytime and nighttime surface heat island intensities, computed as Equations (5) and (6). The day and night SHII were, respectively, derived from the daytime and nighttime LSTs, which subtracts the corresponding mean LST value of non-UF category pixels from the LST value of each pixel in the study region [68]:

$$SHII = average(SHII_{day}, SHII_{night}) \quad (5)$$

$$SHII_{day \text{ or } night} = LST_{urban} - LST_{rural} = LST_i - \overline{LST_{non-UF}} \quad (6)$$

where $SHII_{day}$ and $SHII_{night}$ are the surface heat island intensities for day and night, respectively. LST_{urban} is the LST value of urban pixels, while LST_{rural} indicates the LST value of rural pixels. LST_i denotes the LST value of pixel i within the individual study regions of BTH, GBA, and YRD. The non-UF category pixels are substitutions for rural pixels, encompassing the pixels from various non-UF land cover/use categories. Thus, $\overline{LST_{non-UF}}$ indicates the average LST values of non-UF pixels in the three UAs.

In this study, the yearly average concentration of PM_{2.5} was captured to reflect the air environmental situation and pollution in the three UAs. The values of the yearly average NDVI were used to mirror the environmental comfort and biological health degrees based on green spaces and vegetation situations.

Residential support (RS) refers to the spaces or services arranged for the necessities of human living and life, taking into consideration the land cover/use weights and population density [69]. BTH, GBA, and YRD are the most populated regions in China. Thus, residential support is an essential component of UA's environmental issues. The magnitude of RS in this study was evaluated based on the population distribution and built-up proportion, which is computed using the following equation [69]:

$$RS = Pop_{std} \times P_{BU} \quad (7)$$

where Pop_{std} indicates standardized population density. P_{BU} denotes the built-up proportion derived from the calculation of land cover/use.

2.6. Relationship Profiling

2.6.1. Correlation and Local Bivariate Analysis

Given the data-processing capacity and spatial autocorrelation, we generated a set of 3000 m × 3000 m grid cells as the appropriate analytical scale for the spatial analysis. Thus, this study rescaled the habitat quality and all environmental indicators into 3000 m spatial fishnets for evaluating the relationships and interactions between habitat quality and multifaceted environmental situations. All the spatial operations and modeling in this study were completed in the ArcGIS Pro Version 3.0.1 platform. Initially, we utilized the corrplot R package (under R v4.1.0 statistical software, <https://www.r-project.org/> (accessed on 30 November 2022)) to visualize the correlation matrix for disclosing the global association between various indicators across the entire UA region. Next, we adopted the local entropy model to explore the local connection between habitat quality and various environmental situations.

The local spatial associations between habitat quality and environmental situations were judged based on a local entropy model. The local entropy model is a nonparametric approach proposed by Guo [29] for multivariate data. It integrates local spatial analysis, Rényi entropy calculation, permutation-based distribution estimation, and a set of statistical tests, allowing the interactive detection of significant local multivariate associations over space [29]. Entropy is a gauge for quantifying uncertainties and randomness, such as Rényi entropy and Shannon entropy [29,70,71]. Rényi and Shannon entropies are computed as the following equations:

$$H_\lambda = \frac{1}{1-\lambda} \log \left(\int f(x)^\lambda dx \right) \quad \lambda \geq 0, \lambda \neq 1 \quad (8)$$

$$H = - \int f(x) \log f(x) dx \quad (9)$$

where H_λ indicates Rényi entropy, x denotes a multi-dimensional vector in the data space, $f(x)$ refers to the probability density function, and λ (≥ 0) represents the order of the H_λ . When λ is closing to 1, H_λ converges to the Shannon entropy (H) in the data space [29]. However, the unknown probability density function is the principal challenge when estimating the entropy for exploratory data analysis [29,70,71]. The power-weighted minimum spanning tree (MST) method is an effective alternative for entropy estimation in multivariate data analysis [29]. Accordingly, the local entropy model can be conducted by the following analytical procedures: (1) multivariate Rényi entropy estimation and observation for the local neighborhood, (2) construction for empirical distributions of local joint entropy using permutations based on the null hypothesis and MST method, (3) test for statistically significant local relationships using permutations, and (4) examination and classification of the local relationships [29,70,71]. Notably, using the appropriate parameter values for the size of the local neighborhood and the edge power of the MST is vital in implementing this local entropy model. Specifically, the scaling factor can modulate the sensitivity to subtle relationships. The proper parameter of the neighboring size can improve the likelihood and efficiency of detecting significant relationships and patterns. Additionally, optimizing the number of permutations can permit a neutralization between precision and processing time [29].

The local entropy model proposed by Guo [29] did not assume a prior relationship form, which can estimate multivariate entropy distribution without a probability density function and implement local spatial analysis without a regression model [29]. Thus, there is a growing application of local entropy maps in geography-related studies [29,70–72]. We designed the research steps of local bivariate analysis based on Guo's approach, as shown in Figure 3. The average habitat quality score of each analytical grid was extracted as the dependent variable. The respective average values of SHII, PM2.5 concentration, NDVI, and RS for each analytical grid were estimated as explanatory variable parameters. Further, we conducted a series of local bivariate relationship analyses to investigate the local association between habitat quality and each explanatory variable. We specified a 95% confidence level of the hypothesis test for significant relationships. Six categories of relationships can be identified based on the local entropy model: not statistically significant, positive linear, negative linear, concave, convex, and undefined complex.

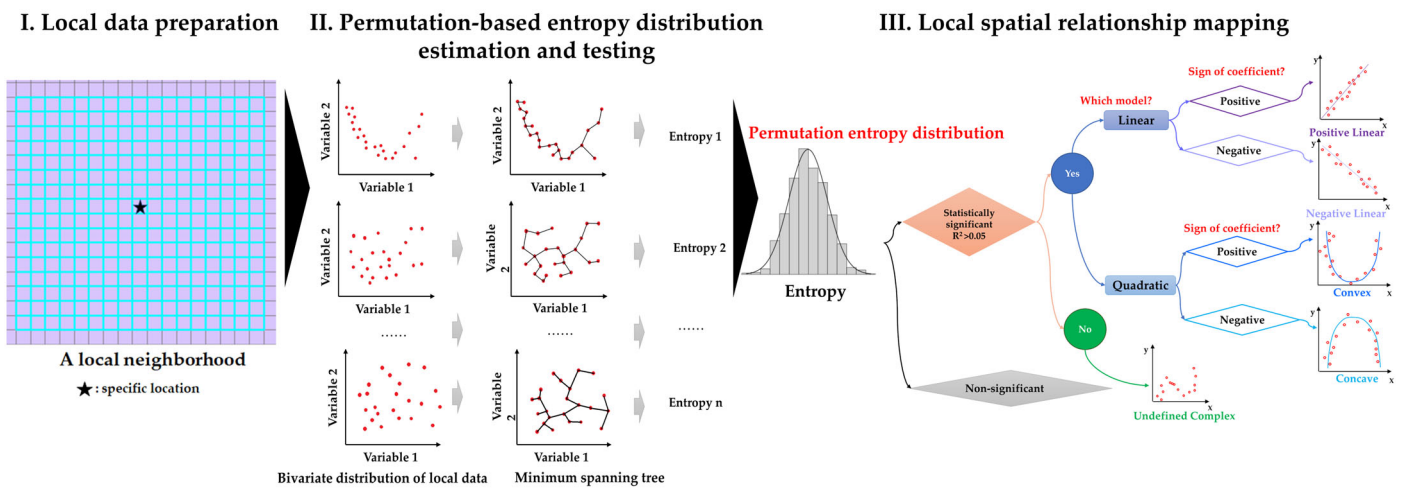


Figure 3. Research flowchart of local bivariate analysis. Note: The flowchart of local bivariate analysis was designed and revised based on Guo’s study [29], consisting of three steps: (I) local data preparation; (II) permutation-based entropy distribution estimation and testing; and (III) local spatial relationship mapping.

2.6.2. Geographical Detector Model

The Geographical Detector Model (GeoDetector) is a novel method for capturing stratified spatial heterogeneity and related driving forces, consisting of risk, factor, ecology, and interaction detectors modules [30,31]. GeoDetector can quantitatively analyze the association and similarity of the spatial distributions between a geostatistical variable and a series of stratified independent variables [31]. The merits of GeoDetector are identifying interaction influences between multiple factors and comparing their differences [31].

The GeoDetector model assumes that the study area is composed of multiple region blocks. Spatial heterogeneity is detected if the total variance of the regions is greater than the sum of the variances of the subregions [31]. In contrast, there is a statistical association between the two variables when the spatial patterns of the two variables tend to be identical [31]. Due to no presuppositions and constraints, the GeoDetector analysis is universal and transplantable [31]. Thus, the GeoDetector model has been used in various research fields, such as the geoenvironmental and sustainability sciences [14,73,74].

Given the consistency of the three UAs, the four numerical indicators—RS, SHII, PM2.5 concentrations, and NDVI—were stratified and categorized using equal intervals classification in conjunction with Jenks natural breaks optimization methods. These four stratified indicators served as the explanatory variables (X) in the GeoDetector analysis. The estimated score of habitat quality was still taken as the dependent variable (Y). Among the four modules of GeoDetector, the risk detector showed the responses of habitat quality on each stratified explanatory variable. The ecological detector was used to examine the significant impact difference of stratified explanatory variables on habitat quality. These two modules can determine the suitable range or type of explanatory variables. However, we were more concerned about the outputs of factor and interaction detectors in this study.

Based on the factor detector module, the magnitude of stratified spatial heterogeneity for habitat quality can be quantified using *q* statistical measures [31].

$$q = 1 - \frac{\sum_{h=1}^L N_h \sigma_h^2}{N \sigma^2} = 1 - \frac{SSW}{SST} \tag{10}$$

where the dependent variable Y (habitat quality in this study) is divided into strata {*h*}, with *h* = 1, . . . , *L*; *N* and *N_h* indicate the number of grids in the whole UA region and strata *h*, respectively; and σ^2 and σ_h^2 denote the variances of the whole region and strata *h*, respectively. *SSW* is the sum of squares within, while *SST* is the sum of squares total. *q* stands for the explanatory power of a specific explanatory variable X (RS, SHII, PM2.5,

and NDVI) for habitat quality, ranging from 0 to 1. The greater the q value, the stronger the influences of the explanatory variable X and the more apparent spatial differentiation of habitat quality [31]. Remarkably, habitat quality exhibits a random spatial distribution when the q value is 0, whereas habitat quality shows complete spatial differentiation when the q value equals 1 [31]. The q value satisfies the non-central F distribution, where λ is the non-central parameter and Y_h is the mean of layer h [31].

$$F = \frac{N-L}{L-1} \frac{q}{1-q} F(\widetilde{L1}, \widetilde{NL};) \quad (11)$$

$$\lambda = \frac{1}{\sigma^2} \left[\sum_{h=1}^L \overline{Y}_h^2 - \frac{1}{N} \left(\sum_{h=1}^L \sqrt{N_h \overline{Y}_h} \right)^2 \right] \quad (12)$$

According to the equations above, the p -value can be calculated as a statistical significance test for the q statistics. The interaction detector module can discern the interactive effect on the habitat quality between two environmental situations. Firstly, the impact (q values) of two stratified environmental situations on habitat quality was estimated as $q(X_i)$ and $q(X_j)$, respectively. Next, we computed the q values of the interactive effect ($q(X_i \cap X_j)$). Ultimately, according to judging criteria (Table 1), the interaction type between two stratified environmental situations can be determined by comparing $q(X_i \cap X_j)$ with $q(X_i)$ and $q(X_j)$. More detailed information on the GeoDetector model can be obtained from the official website (www.geodetector.cn (accessed on 30 November 2022)).

Table 1. Definition of the interaction types in the GeoDetector model [31].

Interaction Types	Judging Criteria	Interaction Relationship Descriptions
Nonlinear-weakened	$q(X_i \cap X_j) < \text{Min}(q(X_i), q(X_j))$	The synergistic effect is nonlinearly weakened by the interplay of two variables.
Univariate-weakened	$\text{Min}(q(X_i), q(X_j)) < q(X_i \cap X_j) < \text{Max}(q(X_i), q(X_j))$	The synergistic effect is univariately weakened by the interplay of two variables.
Independent	$q(X_i \cap X_j) > \text{Max}(q(X_i), q(X_j))$	The effects of individual variables are independent.
Bivariate-enhanced	$q(X_i \cap X_j) = q(X_i) + q(X_j)$	The synergistic effect is mutually enhanced by the interplay of two variables.
Nonlinear-enhanced	$q(X_i \cap X_j) > q(X_i) + q(X_j)$	The synergistic effect is nonlinearly enhanced by the interplay of two variables.

3. Results

3.1. Spatial Characteristics of Habitat Quality Based on Land Cover/Use Evaluation

The thematic maps of land cover/use for three UAs were prerequisites for quantifying the habitat quality, as shown in Figure 4. The UF areas were highly urbanized areas dominated by large-scale built-up areas, highlighted in red. Natural habitat types are presented using different gradients of green and blue. AH referred to a semi-habitat system used for cultivation and farming activities, depicted in yellow.

Upon the completion of the InVEST-HQ analysis, the magnitudes of habitat quality for three UAs in 2015 were assessed, as shown in Figure 5. The habitat quality scores ranged from 0 to 1, representing the worst to perfect ecological situations. We assorted and mapped the habitat quality index into ten levels using an equal interval of 0.1, indicating the lowest (HL1: 0–0.1) to highest habitat quality (HL10: 0.9–1). The habitat qualities of the three UAs and their geographical variations differed by habitat types and suitability. Overall, the habitat situations of the three UAs in 2015 were not optimistic, and approximately one-third of the regions showed low magnitudes of habitat quality (HL1–HL3). The average habitat quality scores in BTH, GBA, and YRD were 0.3563, 0.3399, and 0.3336, respectively. The moderate-quality levels of habitats (HL4–HL6) made up the largest proportion of the three UA regions. However, the high habitat quality areas (HL7–HL10) added up to under 15%

(Figure 5d). The spatial layouts of habitat quality in the three UAs were highly consistent with the configuration characteristics of land cover/use. The scores of non-habitat areas (UF and VL) were estimated to be zero. In contrast, FH and WA showed higher quality scores than other habitat types in the three UAs. However, the habitat quality score of the WA type in GBA was much lower than that of BTH and YRD. There was a large margin of habitat quality score for the GH type between BTH and the other two UAs. The average scores of AH, FH, GH, and WA in 2015 are shown in Figure 6, as these four habitat types dominated the three UAs (over 85% of area shares).

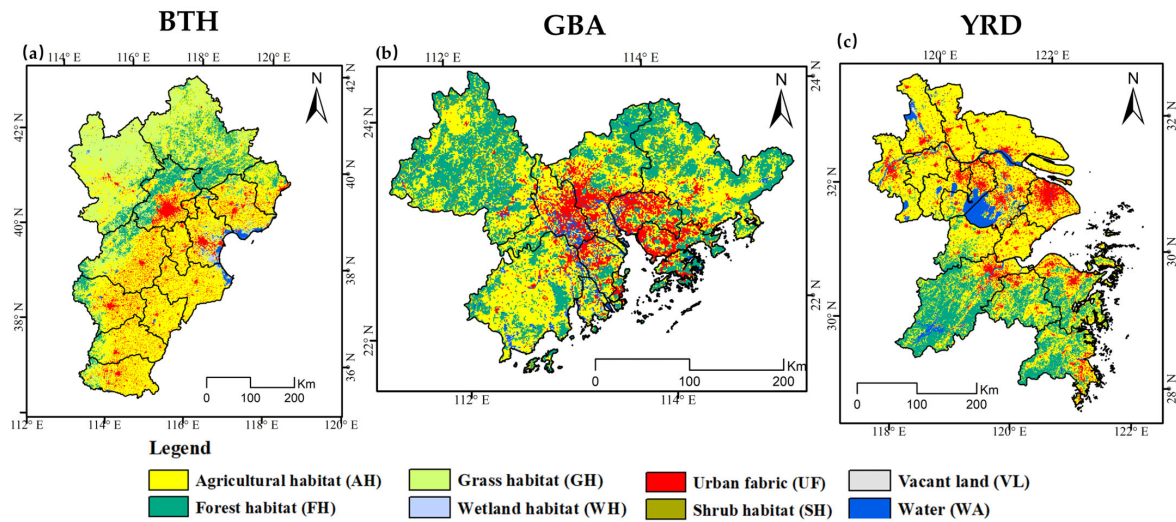


Figure 4. Thematic maps of land cover/use for three UAs: (a) BTH, (b) GBA, and (c) YRD.

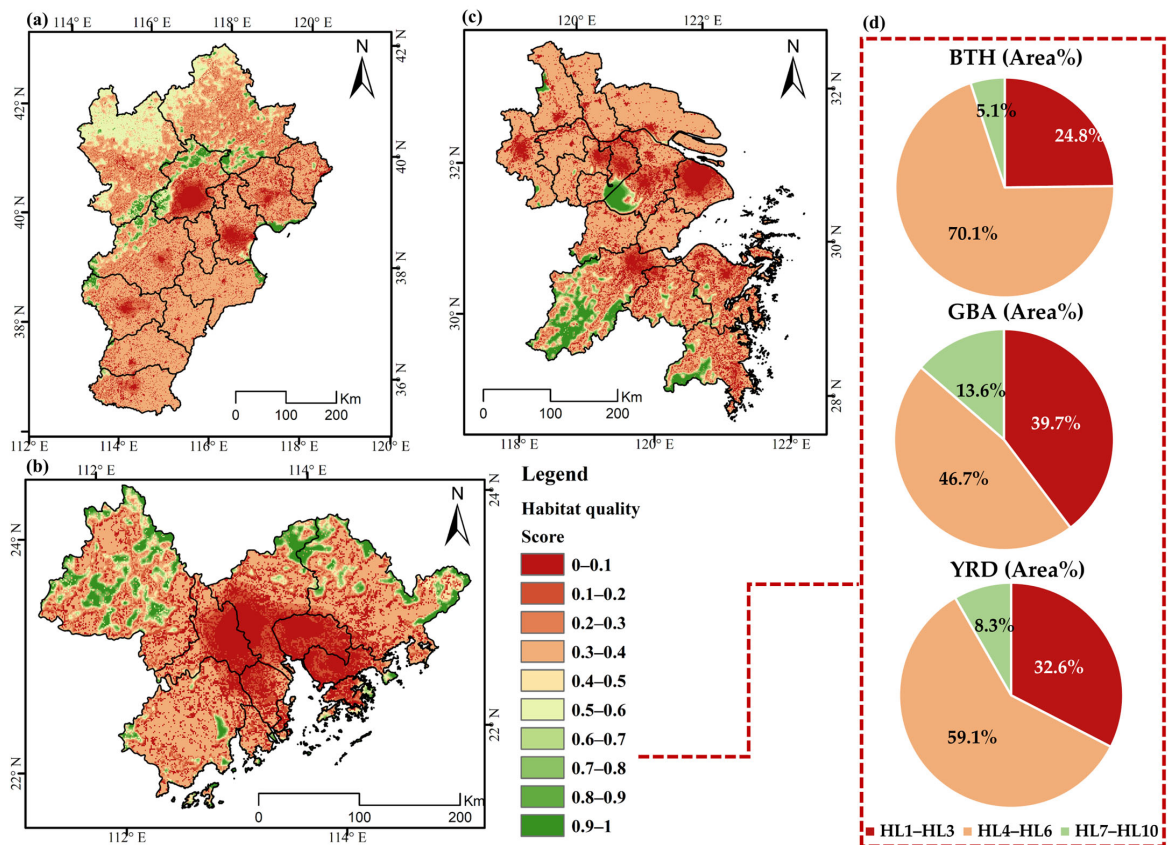


Figure 5. Spatial patterns and distributions of habitat quality in the three UAs: (a) BTH, (b) GBA, (c) YRD, and (d) area summary.

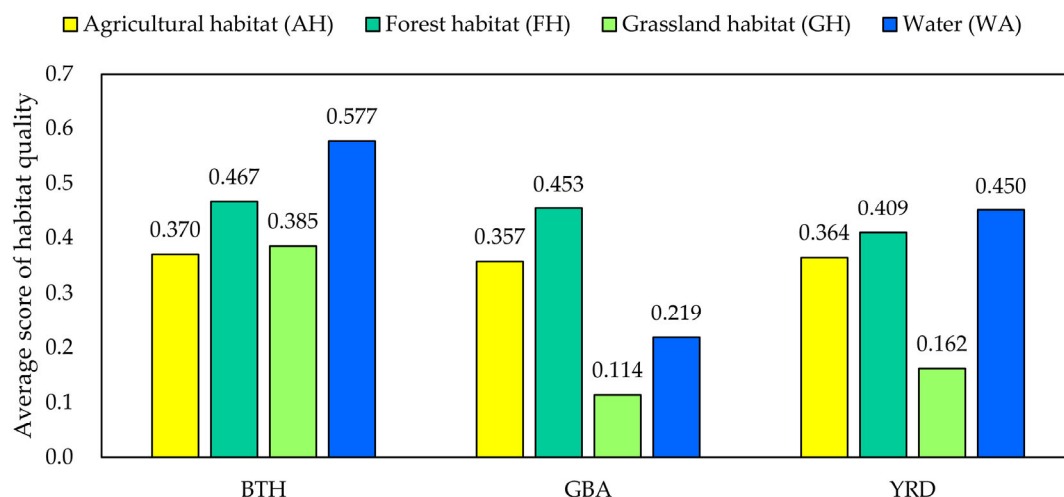


Figure 6. The scores of habitat quality for the four dominant land cover/use.

Geographically, the areas with low habitat suitability in the three UAs in 2015 were chiefly located in human settlements, namely, urban and peri-urban fringes, indicating the adverse influences of anthropogenic activities on the regional habitats. The northwest part of BTH showed high-quality scores due to mountain ridges and massive forests, while the most serious habitat fragile areas were detected in Beijing and Tianjin. The severe habitat delicate areas in GBA were roughly configured as a triangle-shaped region, extending from Guangzhou–Foshan outwards to Macao, Zhuhai, Shenzhen, and Hong Kong. Only Zhaoqing and Huizhou exhibited favorable circumstances for habitats due to their abundant natural capital. In YRD, the southern part and the Taihu region were prominent due to their superior habitat suitability. Shanghai, the south of the Jiangsu Province, and the north of the Zhejiang Province suffered from a challenging habitat situation in 2015 due to the sparse vegetation availability.

3.2. Spatial Stratification of Multi-dimensional Environmental Situations

Although the annual LST values showed a large difference in tendency and influence depending on the day and night, the spatial patterns of day and night heat island intensities in the three UAs were highly consistent. In light of this, this study utilized the mean value of yearly daytime and nighttime SHII to reflect the regional comprehensive thermal environment status in the three UAs. The spatial arrangements of daytime and nighttime thermal environments (both LST and SHII) in the three UAs are shown in the Supplementary Materials. This study divided the SHII index into five categories: ≤ 0 , $0\sim 1$, $1\sim 2$, $2\sim 3$, >3 (unit: $^{\circ}\text{C}$, Grades I–V) (Figure 7). The 2015 average values of daytime LST in BTH, GBA, and YRD were estimated to be 19.99°C , 24.7°C , and 20.83°C , respectively, and those of respective nighttime LST were 21.84°C , 26.79°C , and 22.67°C . The non-habitat areas and agricultural habitats dominated the areas with high SHII values. The area ratios of positive SHII regions were 56.36% in BTH, 57.12% in GBA, and 60.51% in YRD.

Significant spatial differentiations of yearly average PM_{2.5} concentrations were found in the three UAs. The spatial maps of the average PM_{2.5} concentrations in 2015 for the three UAs were stratified into five categories: ≤ 30 , $30\sim 40$, $40\sim 50$, $50\sim 60$, >60 (unit: $\mu\text{g}/\text{m}^3$, Grades I–V), as shown in Figure 8. The BTH regions showed the worst air condition among the three UAs, and about 43.78% of the regional territory was exposed to severe air pollution (Grade V). Most of the GBA regions (94.26%) in 2015 were clustered in Grade II and III PM_{2.5} concentrations. Only 13.8% of YRD regions did not suffer from severe air pollution.

This study weighed the UAs' living supporting capacity based on the product of built-up proportion and population density. Regions without living supporting capacity were assigned the value of zero. The RS value was equal to one, indicating perfect resi-

dential suitability. We defined five grades for the RS index: 0 (without RS capacity), 0~0.1, 0.1~0.2, 0.2~0.3, >0.3 (unitless, Grades I–V). There were multiple cores with extremely high living supporting capacity in the three UAs, as shown in Figure 9. Regions with residential suitability in BTH, GBA, and YRD were estimated to be 26.75%, 26.27%, and 30.1%, respectively.

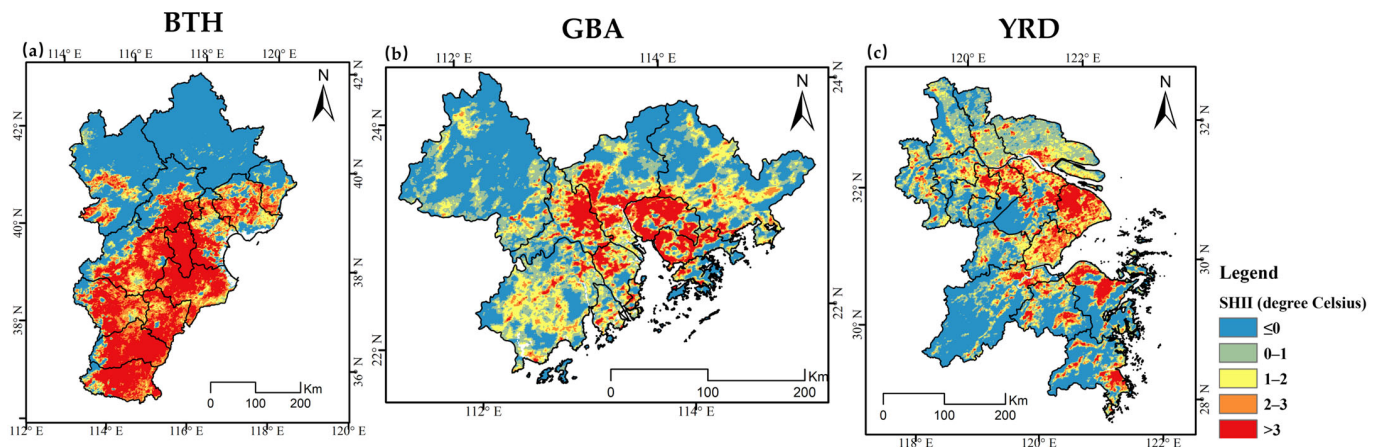


Figure 7. Spatial stratification of the thermal environmental situations in the three UAs: (a) BTH, (b) GBA, and (c) YRD.

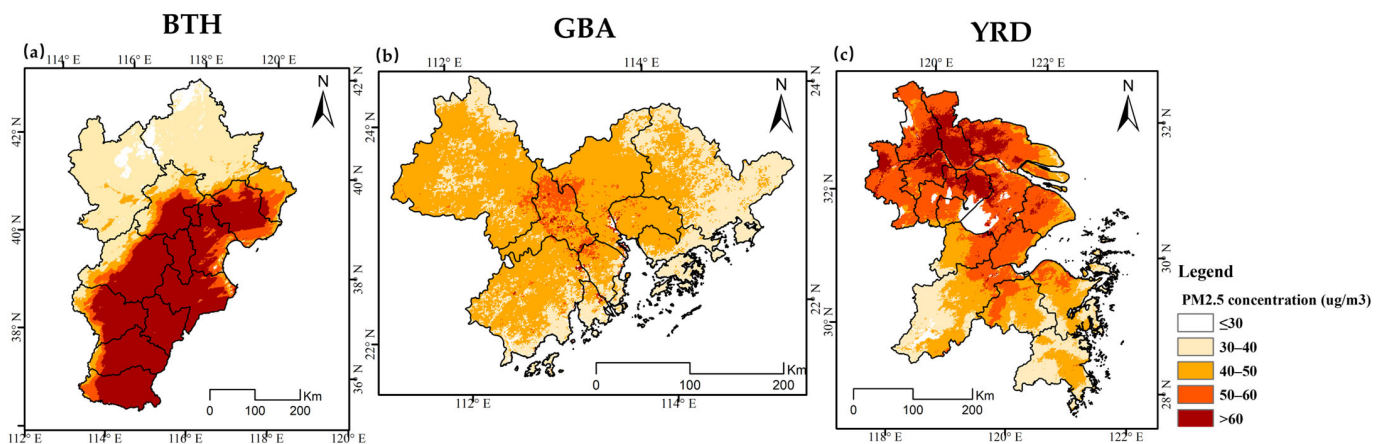


Figure 8. Spatial stratification of the air environmental situations in the three UAs: (a) BTH, (b) GBA, and (c) YRD.

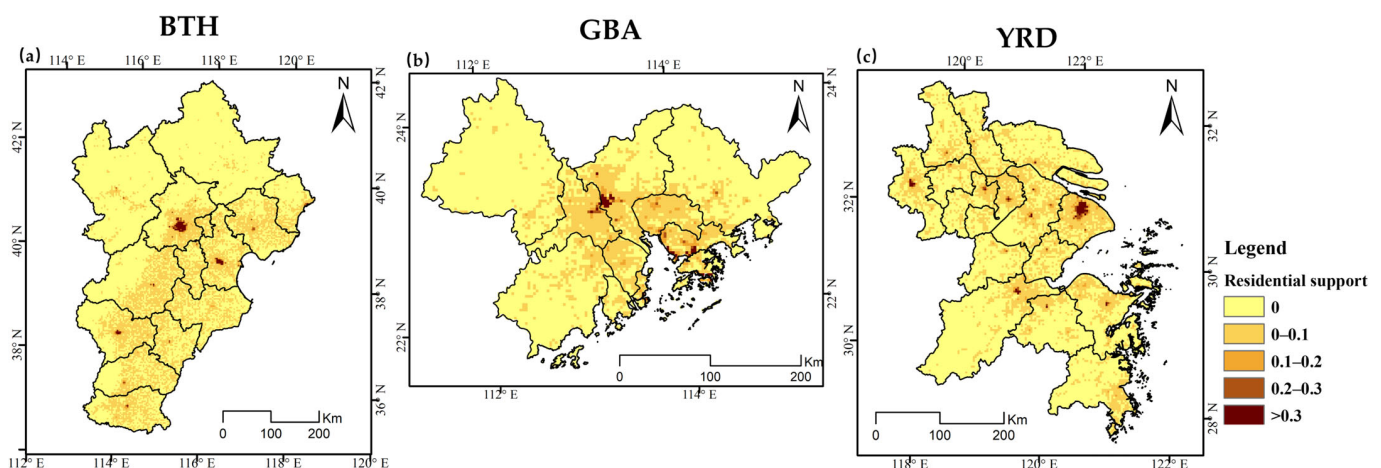


Figure 9. Spatial stratification of the residential situations in the three UAs: (a) BTH, (b) GBA, and (c) YRD.

NDVI represents the aesthetic, recreational, and regulating functions of natural landscapes. We mapped the spatial patterns of the NDVI index with an interval of 0.2 for the three UAs (unitless, Grades I–V, Figure 10). In 2015, the average values of NDVI were projected to be 0.7263 in BTH, 0.7196 in GBA, and 0.6798 in YRD. Approximately 84.77% of BTH regions, 75.33% of GBA regions, and 72.30% of YRD regions had high values of NDVI, exceeding 0.6 in 2015.

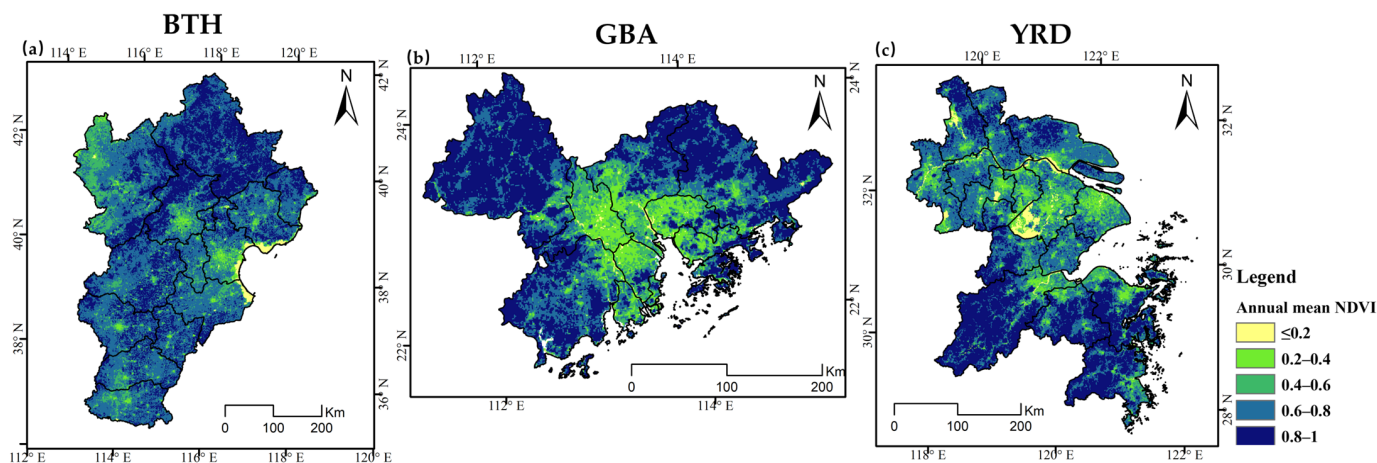


Figure 10. Spatial stratification of the biological health situations in the three UAs: (a) BTH, (b) GBA, and (c) YRD.

3.3. Correlations of Environmental States

We started with the correlation analysis between habitat quality and four environmental status indicators. In general, three UAs exhibited identical relation patterns in the entire regional scale, albeit with varying degrees. Habitat quality in the three UAs was negatively associated with the indicators of SHII ($R^2 \geq 0.49$, $p < 0.001$), PM2.5 concentrations ($R^2 \geq 0.38$, $p < 0.001$), and RS ($R^2 \geq 0.26$, $p < 0.001$), while positively related to NDVI ($R^2 \geq 0.3$, $p < 0.001$). The correlation coefficients between habitat quality and SHII were the highest in GBA ($R^2 = 0.73$) and the lowest in BTH ($R^2 = 0.49$). The association between habitat quality and NDVI degrees in GBA ($R^2 = 0.62$) was the strongest among the three UAs. The most salient impact of PM2.5 concentrations ($R^2 = 0.44$) on habitat was detected in BTH. YRD showed the highest coefficient between habitat quality and RS ($R^2 = 0.32$). As for the four environmental status indicators, there were positive correlations among SHII, PM2.5 concentration, and RS, but NDVI negatively varied with other indicators ($p < 0.001$). In terms of UA, the strongest associations were SHII–PM2.5 concentration in BTH ($R^2 = 0.81$) and SHII–NDVI in GBA ($R^2 = 0.74$) and YRD ($R^2 = 0.64$). In contrast, there were minor linkages between PM2.5 concentrations and RS in all the studied UAs ($R^2 \leq 0.12$). The relevant correlation coefficients are shown in Figure 11.

We identified six types of spatial structural relationships between habitat quality and four environmental status indicators based on the local entropy model. We assumed that there were local relationships between quality and individual environmental status indicators in the three UAs under the 95% confidence level. We set the 0.5 scaling factor, 30 neighborhoods, and 199 permutations to perform the hypothesis test for accommodating local spatial relationships.

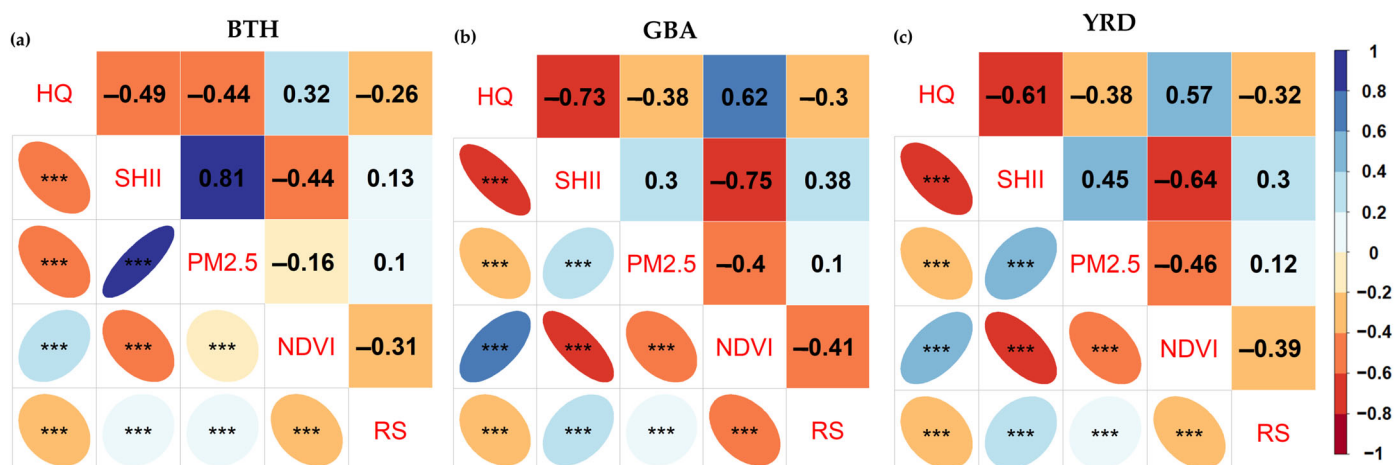


Figure 11. Correlograms of multifaceted environmental situations in the three UAs: (a) BTH, (b) GBA, and (c) YRD. Note: The asterisk symbols (***) are representative of the statistical significance at the 0.1% level ($p < 0.001$).

The relationships were predicted and determined based on the adjusted R-square and the model's Modified Akaike Information Criterion (AICc). The classified local relationships in the three UAs are mapped in Figure 12, and the relevant categorical summary is shown in Table 2. We provided the entropy statistic and detailed information on the local bivariate analysis in the Supplementary Materials. The results of the local bivariate analysis displayed local structural relationships of various forms between habitat quality and environmental situations over space. Furthermore, the generated maps of local bivariate analysis differentiated the significance levels within a certain neighboring extent. Many regions showed statistically non-significant relationships in the local contexts of the three UAs, indicating a spatially random distribution pattern between variables presented in these regions. The spatially explicit local relationship maps provided an overview of the spatial diversities for significant local associations between habitat quality and environmental situations and navigated the analysis to focus on specific areas. The local bivariate analysis, thus, offered considerable interpretation clues. For example, about 4.86% of BTH regions showed a concave relationship between habitat quality and SHII, indicating that habitat quality in the corresponding BTH regions followed a concave curve as the SHII varied.

We found that the total area ratios of linear and quadratic models for the HQ–SHII relationship in BTH were 23.95% and 10.59%, respectively. This finding indicates that the polynomial and linear models can explain the 23.95% and 10.59% relationship between habitat quality and thermal environment in BTH, respectively. These explanations were also suitable for other estimated coefficients. Thus, the local bivariate analysis allowed us to capture the extent of local heterogeneity between habitat quality and different environmental situations: 27.37–43.14% in BTH, 23.7–65.37% in GBA, and 27.95–55.84% in YRD.

Comparing the performance of four environmental situation indicators, the spatial influences of SHII, NDVI, and RS on habitats in the neighboring local setting were more apt to be detected. However, understanding how the PM2.5 concentration locally influenced the UAs' habitat over space was not completed due to there being over 72% of non-significant areas. Looking at the statistically significant features, the negative linear relationship accounted for the largest share in the HQ–SHII, HQ–PM2.5, and HQ–RS results. In contrast, the positive linear relationship was the most remarkable in the HQ–NDVI results.

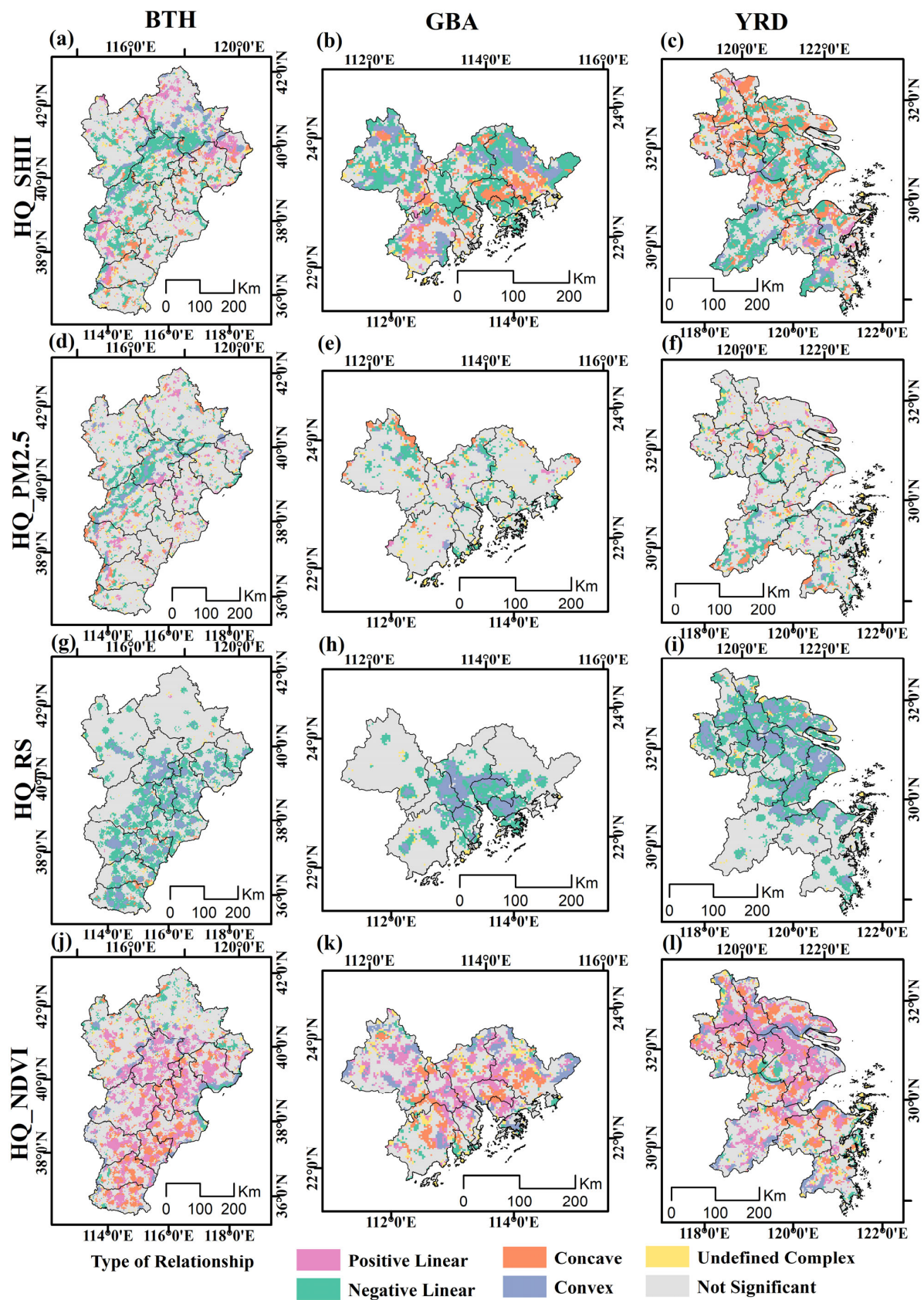


Figure 12. Local spatial relationship between habitat quality and multifaceted environmental states: (a–c) HQ–SHII for BTH, GBA, and YRD, respectively; (d–f) HQ–PM_{2.5} for BTH, GBA, and YRD, respectively; (g–i) HQ–RS for BTH, GBA, and YRD, respectively; and (j–l) HQ–NDVI for BTH, GBA, and YRD, respectively.

Table 2. Categorical summary of the local bivariate analysis.

BTH				
Type of Relationship	HQ–SHII	HQ–PM2.5	HQ–RS	HQ–NDVI
Positive Linear	6.99%	4.62%	0.11%	20.87%
Negative Linear	16.96%	10.47%	21.16%	4.27%
Concave	4.86%	3.77%	1.00%	9.87%
Convex	5.73%	4.56%	10.44%	5.48%
Undefined Complex	3.89%	3.95%	1.15%	2.66%
Not Significant	61.57%	72.63%	66.15%	56.86%
GBA				
Type of relationship	HQ–SHII	HQ–PM2.5	HQ–RS	HQ–NDVI
Positive Linear	4.17%	1.35%	0.01%	16.91%
Negative Linear	30.17%	10.48%	16.50%	4.78%
Concave	11.53%	3.23%	0.03%	9.28%
Convex	12.26%	1.91%	10.01%	10.81%
Undefined Complex	7.25%	6.72%	2.25%	7.43%
Not Significant	34.63%	76.30%	71.20%	50.80%
YRD				
Type of relationship	HQ–SHII	HQ–PM2.5	HQ–RS	HQ–NDVI
Positive Linear	4.16%	3.20%	0.01%	22.00%
Negative Linear	21.41%	11.36%	27.99%	5.46%
Concave	16.18%	4.08%	0.30%	11.43%
Convex	6.23%	2.11%	16.86%	10.53%
Undefined Complex	5.65%	7.20%	3.37%	6.42%
Not Significant	46.36%	72.05%	51.47%	44.16%

3.4. GeoDetector-Based Interactive Effects Assessment

Spatial stratified heterogeneity and interactive influence between habitat quality and multi-dimensional environmental status in the three UAs were captured using GeoDetector. The outputs show that the geographically stratified heterogeneities of habitat quality in the three UAs were, to a certain extent, affected by multifaceted environmental status. The habitat quality varied significantly over space for each graded environmental status indicator based on a series of *t*-tests at a significance level of 0.05. The related outputs of factor and ecological detector modules are shown in the Supplementary Materials. The stratified average values of habitat quality in each stratum of environmental situations for the three UAs are shown in Figure 13. The *q* statistic coefficients for four graded environmental status indicators in the three UAs under the factor detector module are shown in Figure 14. The higher *q* statistic coefficient indicated a greater explanatory power for the stratified heterogeneity of habitat quality. According to the coefficients of the *q* statistic, the most crucial influencing indicators on habitat quality in the three UAs were PM2.5 concentration (BTH, $q = 0.17$), SHII (GBA, $q = 0.30$), and NDVI (YRD, $q = 0.21$). Other indicators also showed a considerable impact on habitat quality. The outputs of the interaction detector module revealed the interactive influences from a combination of multiple environmental status indicators on habitat quality, as shown in Figure 15. With reference to the judging criteria of interaction (Table 1), we found that the *q* statistics for the bivariate interactions were greater than the *q* statistics for every single factor, indicating that the explanatory power of a single indicator could be mutually enhanced when interacting with another one. The cumulative effects of different environmental statuses could bring about more pressures and risks on habitat quality. Specifically, in BTH, the PM2.5 concentration played a dominant role in the single-factor influence analysis and strongly interacted with other indicators. The predominant interaction between PM2.5 concentration and NDVI showed the highest *q* statistic. A similar phenomenon was also found in the SHII indicator of GBA and the NDVI indicator of YRD.

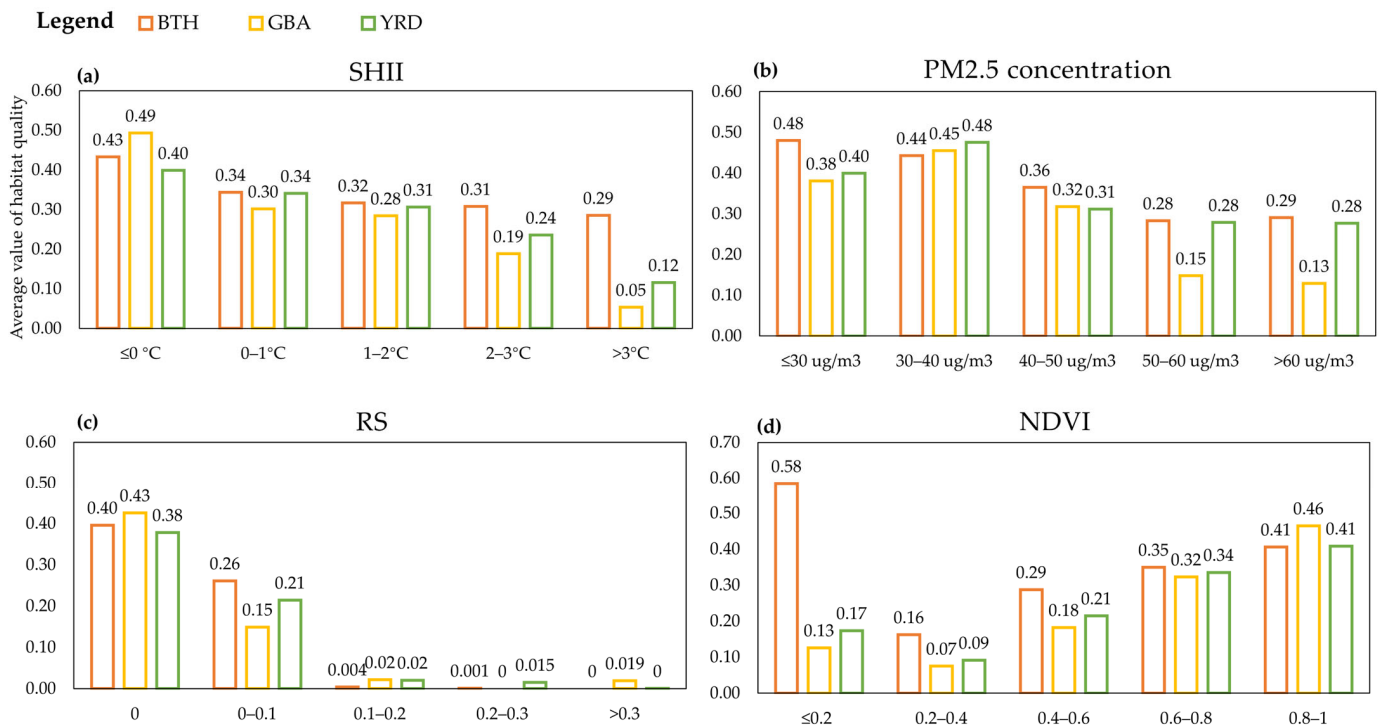


Figure 13. The performances of the graded environmental situations under the risk detector: (a) SHII, (b) PM2.5, (c) RS, and (d) NDVI.

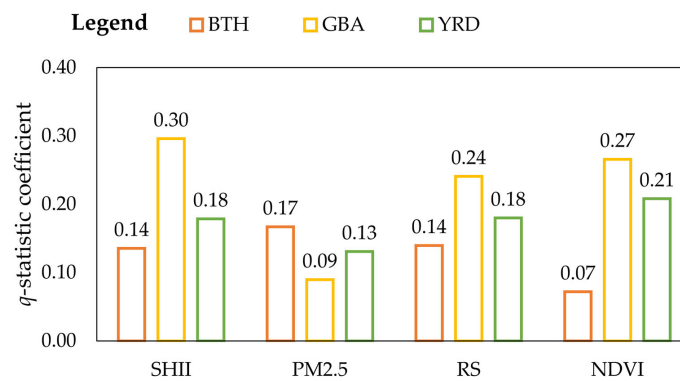


Figure 14. The q -statistic coefficients for the grading indicators in the three UAs.

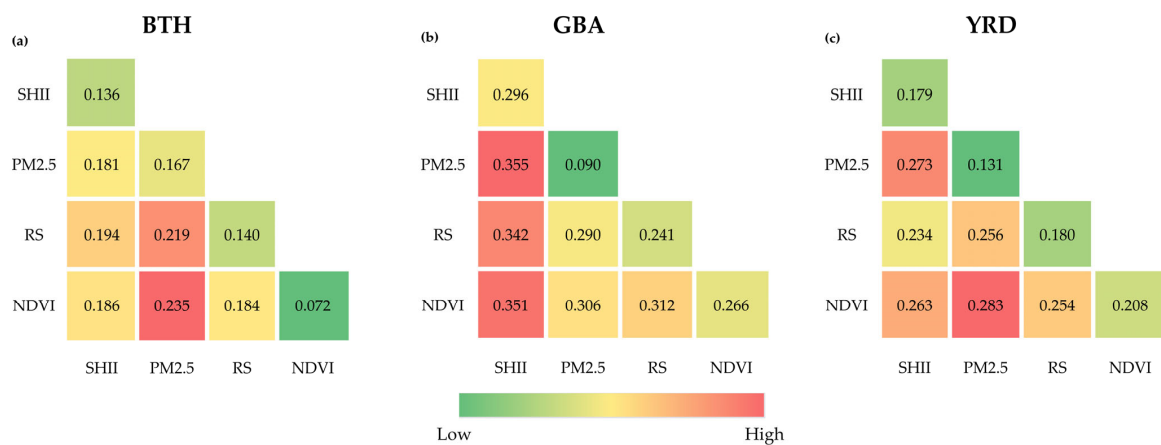


Figure 15. Interactive influences of different environmental situations on habitat quality: (a) BTH, (b) GBA, and (c) YRD.

4. Discussion

4.1. The Impacts of Multifaceted Environmental States on Habitat Quality in the Three Urban Agglomerations

Focusing on BTH, GBA, and YRD, this study spatially evaluated the relationships between habitat quality and multifaceted environmental states using various methods. The cartographic comparison allowed us to capture spatial differentiation and hotspots, the correlation analysis provided a global overview of the statistical relationships, the local entropy model inspected the local structural associations, and GeoDetector identified the spatial stratification heterogeneity and interactive influence. Through such incorporation of multi-perspective profiling, this study presents a comprehensive panorama of the interconnection of various environmental circumstances and their impacts on habitats for different UAs. As a series of biophysical and anthropogenic drivers can threaten the habitat quality and simultaneously trigger changes in different environmental mechanisms, there were similarities and discrepancies in the performances of the three UAs, reflected by the dominant impact and relationship strengths.

Based on the overlay of habitat quality and land/cover use maps in the three UAs, we found that more than four-fifths showed low–medium habitat suitability, spatially clumped in the human settlement and cultivation areas. Meanwhile, large-scale UF areas displayed prominent heat island phenomena, terrible air quality, over-intensive living space, and sparse green availability, albeit with varying degrees of three UAs. Habitat types with high greenness (e.g., forests) in the three UAs showed small gaps in habitat quality scores, ranging from 0.409 to 0.467. The scores of habitats with low greenness (e.g., grass, water) greatly varied across different UAs, depending on habitat types and extents (Figures 6 and 13d). Grounded on correlation analysis, SHII, PM_{2.5} concentrations, and RS showed an overall deteriorative impact, whereas NDVI had a beneficial influence on the habitat quality in the three UAs. This result was in line with previous environmental-related studies [10,14,15,44,49,74,75]. We also recognized that the most noticeable impacts on habitat were air pollution in BTH, thermal stress, and green capacity in GBA, and residential pressure in YRD. Thus, habitat quality tied in closely with natural assets' situations, indicating that habitat-related strategies depended on improving and maintaining the green and blue spaces.

Next, bivariate relationship profiling based on the local entropy model identified and delineated the local spatial influence of individual environmental status on habitat quality. The spatial mapping of local relationships showed the advantage of distinguishing diverse types of significant associations and highlighting their spatial patterns. Local spatial relationships were roughly in agreement with the global trend of the entire UA. Except for non-significant areas, the habitat quality scores of most regions in the three UAs were negatively related to SHII, PM_{2.5} concentrations, and RS, while positively associated with NDVI at the 95% confidence level. The local spatial influences of different environmental statuses on habitats were complicated with a rich mixture of relationship types, regardless of UAs. However, large shares of non-significant areas emerged in terms of HQ–PM_{2.5} (>72%) and HQ–RS (>51%). The PM_{2.5} concentrations used in this study were estimated based on in situ observations, AOD distribution, and auxiliary data (e.g., land cover/use and population) [57,58]. Our habitat quality scores were assessed using the land cover/use-based InVEST–HQ module [60]. It is difficult to simulate the habitat suitability and quality considering air-related threats due to model constraints, which interfere with the relationships captured between habitat and PM_{2.5} concentrations. Regarding HQ–RS performance, the non-significant areas mainly belonged to natural habitats without residential function and service.

The upshots from GeoDetector analysis generally conformed with the foregoing paired relationship profiling and demonstrated the pile-up effect of any two different environmental issues. Relying on the GeoDetector investigation, this study emphasized spatial differences in the overlapping effects and interaction relationships of differently graded environmental strata on habitat quality. Using the interaction detector, we figured out that the impacts of the combination of different environmental issues on habitats in the

three UAs were bivariate-enhanced rather than independent or weakened, indicating the aggravation and amplification of compound effect compared with the influence of a single environmental status. In terms of the BTH region, the cumulative effects of air pollution in conjunction with other environmental issues were more severe, coinciding with previous investigations [57,76,77]. BTH has struggled with the worst consequences of air pollution due to a chain of factors [16,78–80]. BTH is the national capital region of China, with over 110 million people [45]. The primary contributors were high energy consumption, vehicle emissions, biomass burning, and neighboring heavy industries [79,80]. As surrounded by mountains, BTH was a victim of its topography, where pollutants are trapped within the regional limits (mainly in the south and east of BTH).

In contrast, the overlapping influences of the heat island phenomenon and other issues in GBA have attracted more attention. We identified that the average annual daytime and nighttime LST values in GBA were the highest among the three UAs. On the other hand, a vast extent with low habitat quality scores in GBA was spatially congregated in the three contiguous megacity clusters (Dongguan–Guangzhou–Foshan, Zhuhai–Macao, and Shenzhen–Hong Kong). Meanwhile, these three contiguous megacity clusters exhibited forceful residential service capacities and low green gradients. However, GBA was superior to the other two UAs in the scale, extent, and gradient of air pollution. Most areas with over 50 $\mu\text{g}/\text{m}^3$ annual PM_{2.5} concentrations in GBA were merely spatially distributed in Foshan. Accordingly, we observed the lowest impact of PM_{2.5} concentrations on GBA's habitats. In the YRD case, the interactions between NDVI and other indicators stood out. Additionally, there were minor gaps in impact magnitudes between indicators for YRD in comparison to those for BTH and GBA. We noticed that the gradient of NDVI and habitat quality in YRD were inferior to that of the other two UAs. These performances of YRD can be partly ascribed to development gradients and geomorphic features. Owing to the fast-growing urban built-up and settlements in recent decades, YRD is the most populated, urbanized, and prosperous region in China, with numerous megacities and more than 80 million urban dwellers [45]. Most areas of YRD render a plain terrain, whereas uplands and forests are spatially configured in the south region. Shanghai, Hangzhou Bay, and Suxichang Metropolitan Areas are the most remarkable regions with high urbanness. Such geographical configuration of YRD could respond to its layout and composition of habitat quality, revealing the lag and importance of YRD's greenness and habitat security.

4.2. Road Ahead and Implication for the Spatial Management of Multi-Dimensional Environmental Issues

The uniqueness of this study was the multi-perspective profiling of numerous environmental issues and their interactions. Unlike other environmental studies, this study discerned the associations and interactive effects of different environmental situations instead of clarifying the mechanisms and driving forces of individual environmental problems. Initially, the circumstances of the designated onefold environment in the three UAs were separately evaluated using different indicators and methods. Subsequently, we constructed an integrated framework that combined multiple approaches to link the varying mixes and degrees of different environmental impacts on habitats. This framework propels the multi-objective sustainable management of natural-social capital and co-benefits-seeking policies.

The spatially explicit quantification, mapping, and profiling of various environmental impacts and their relationships serve as the chief references for development plans and policymaking. In recent years, numerous studies detected trade-offs and synergies among multiple environmental services, demonstrating how to move towards sustainability by optimizing the governance and service deliveries of different ecosystems [24,81]. Analogously, our understanding of multifaceted environmental situations and their influences on habitat quality can support work toward tailored sustainable pathways to specify (1) whether and where to adopt the countermeasures to safeguard nature and human habitats, (2) which sector and whose situation should be accounted for and take the corresponding precedence,

and (3) how to reduce overlapped risks and advance the co-benefits, which we examined in the context of the three largest Chinese UAs.

Our evaluation results for these three UAs suggest the weightiness of embracing the spatial diversities and context heterogeneities of regional environmental situations for spatially targeted decision-making. Importantly, the landscapes delivering high habitat quality (score ≥ 0.7) in the three UAs occupied only under 15% of their respective areas. However, over half areas emerged with varying strengths of deteriorative environmental consequences across different aspects. This study focused on four environmental issues, namely, heat-related stress, air pollution, over-intensive living space, and limited urban afforestation, which have been the most common and urgent problems in UA regions and emphasized in national initiatives and local policies [23,25]. We identified that the compound impacts were amplified when one environmental issue overlapped with another. Since the interactive effects of different environmental issues were not independent, strategies to improve an onefold environment may contribute to ameliorating other environmental situations. It is imperative to take advantage of the interactive traits of environmental issues to safeguard and advance regional sustainability, preventing the formation and magnification of multifold risks from ecological, climate, and social aspects.

Furthermore, the motivation for UA formation is integrating regional resources, complementarity advantages, and beneficial cooperation [6]. The geographical heterogeneities and multi-dimensional gaps of UAs can offer opportunities for establishing rational resource allocation and cost-sharing mechanisms [6]. The core megacities and highly populated areas of the UA have been subjected to multiple environmental pressures. Due to the extremely constrained habitat availability and ecological carrying capacities, the supply of essential ecological services in these areas should be addressed by the enrichment and complementary of surrounding natural/semi-natural ecosystems rather than self-sufficiency [82]. Therefore, it is crucial to review the heterogeneities and relationships of the multifaceted environmental situations across the entire UA. By synthesizing different situations, the corresponding geographic areas should be identified to efficiently demarcate vulnerable environmental zones, implement the scopes of mitigation or restoration, and equitably assign environmental compensation [24,82].

Considering different hotspots and relationships between environmental issues, the spatial targeting of specific policies should be deliberated in potentially vulnerable areas to ensure effectiveness [38,83,84]. Spatially explicit mapping should visualize the performance of habitat quality and various environmental states, which can be more prone to identifying corresponding vulnerable locations. The most suitable strategies should be generated by integrating the different environmental profiles and minimizing overall negative feedback [23]. For example, since the most severe problem in BTH is air pollution, the interaction between air pollution and other issues can be aggravated. The mitigation of air pollution should be a considerable priority [19,79,80]. A series of strategies and interventions, including a clean energy plan, vast investments in urban greenery, the optimization of energy consumption structure and efficiency, and technological innovations [53], can take precedence to ameliorate the pollution condition of BTH. Simultaneously, thermal and biophysical environments in BTH can also be improved due to common management strategies. Similar arguments are suitable for GBA and YRD. A relief of the heat island phenomenon in GBA and the management intervention of urban afforestation in YRD should take precedence. Prioritization of decision-making in tandem with compound risk minimization sheds light on a promising amelioration pathway of both onefold and comprehensive UA environments, which can make the achievements of spatially comprehensive management and multi-dimensional sustainability possible and efficient from various aspects [19,23,82].

Although we are confident about the contributions of this study to sustainability-related policymaking processes, there is still enormous potential for our framework. Firstly, we are considering the improvement of the habitat quality quantification in further studies by incorporating more threat source data and models, such as traffic data and heavy

industrial zone. Our habitat quality was mainly derived from land cover/use evaluation and, to some extent, affected the investigation of relationships between habitat quality and certain environmental situations (e.g., air quality). On the other hand, there can be a dynamic improvement when updating the indicators of environmental issues from a spatiotemporal perspective. In this study, restricted by data availability and consistency, we only evaluated the situations and impacts of four environmental issues on the spatial grid scale in 2015. The relationships between environmental issues and their influences may vary across different spatial scales and evolve over time. We desire to add more temporal dynamics and incorporate policy information to verify the proposed comprehensive research framework further. In particular, significant spatiotemporal disparities and trends may be reflected when comparing the situations before and after the COVID-19 pandemic. Moreover, we can endeavor to explore more environmental issues to enrich the multifaceted evaluation. Environmental profiles, such as energy emission, water purification, and food security, can be synthesized into our future research framework to produce more insights for sustainability support.

5. Conclusions

In tailoring sustainable development schemes for the three UAs of BTH, GBA, and YRD, we profiled the relationships and interactions between habitat quality and multi-environmental status indicators from various perspectives by integrating cartographic comparison, correlation analysis, local entropy map, and GeoDetector. The cartographic comparison highlighted geographical hotspots, the correlation analysis weighed global heterogeneities, the local entropy map differentiated the local spatial associations, and GeoDetector recognized interactive relationships.

The contributions of this study stem from four aspects: (1) spatial valuation of habitat quality for the three UAs; (2) spatial overview of the multifaceted environmental situations for the three UAs; (3) multi-perspective profiling of the relationships and interactive influences of different environmental situations on habitat quality for the three UAs; and (4) implications for supporting habitat sustainability and co-benefit-sought decisions. The critical discoveries are summarized as follows:

In 2015, most of the regional landscapes in the three UAs delivered low/medium habitat availability levels overlapped with threats from the thermal, air, living, and biological environmental spheres. The worst compound environmental risks were geographically aggregated in highly urbanized areas, showing an execrable habitat quality. As expected, the habitat security of the UAs was diminished by the heat island phenomenon, air pollution, and residential support. In contrast, enhancing afforestation in the UAs can be a promising pathway to maintain habitat health. The delineation of the local structural relationships between habitat quality and different environmental statuses highlighted the spatial complexity of the influences and interplay among various environmental systems, indicating potential environmental injustice, spatially heterogeneous changes, and context dependency. Strategies targeting specific environmental issues may induce spatially varying consequences on habitats and produce various trade-offs in other environmental systems. The interaction between various environmental issues manifested bivariate-enhanced effects, implying that the overlay of different environmental issues can magnify the influence of each environmental risk. The seriousness of the worst environmental issue would deteriorate when overlapping with others. Thus, the prioritization of decision-making processes may be required in different geographical contexts, such as air pollution removal in BTH, heat island mitigation in GBA, and green space improvement in YRD.

In conclusion, the findings of this study support the multi-dimensional sustainability and co-benefits sought by taking advantage of the relationships and interactions between habitats and diverse environmental issues in the UAs.

Supplementary Materials: The following supporting information can be downloaded at: <https://www.mdpi.com/article/10.3390/rs15040921/s1>, Table S1. Threat parameter settings for estimating habitat quality; Table S2. The sensitivity parameter settings of habitat types to threat factors; Table S3. Entropy results summary for local bivariate analysis; Figure S1. Spatial stratification of the land surface temperatures (LSTs) in the three UAs; Figure S2. Spatial stratification of the surface heat islands in the three UAs; Figure S3. Results for ecological detector module; Figure S4. Results for risk detector module.

Author Contributions: Conceptualization, F.L. and Y.M. (Yuji Murayama); Data curation, F.L.; Formal analysis, F.L.; Funding acquisition, Y.M. (Yuji Murayama); Investigation, F.L.; Methodology, F.L.; Project administration, Y.M. (Yuji Murayama); Resources, F.L., Y.M. (Yuji Murayama) and Y.M. (Yoshifumi Masago); Software, F.L.; Supervision, Y.M. (Yuji Murayama); Validation, F.L.; Visualization, F.L.; Writing—original draft, F.L.; Writing—review and editing, Y.M. (Yuji Murayama) and Y.M. (Yoshifumi Masago). All authors have read and agreed to the published version of the manuscript.

Funding: This research was partly supported by the Japan Society for the Promotion of Science (JSPS) grants of 21K01027 and 18H00763.

Data Availability Statement: The data that support the findings of this study are available upon reasonable request from the corresponding author.

Acknowledgments: The authors highly appreciate the editors and anonymous reviewers for their valuable and constructive comments and suggestions to improve the manuscript.

Conflicts of Interest: The authors declare no conflict of interest.

References

- IPCC. *Climate Change 2022: Impacts, Adaptation, and Vulnerability. Contribution of Working Group II to the Sixth Assessment Report of the Intergovernmental Panel on Climate Change*; Pörtner, H.-O., Roberts, D., Tignor, M., Poloczanska, E., Mintenbeck, K., Alegría, A., Craig, M., Langsdorf, S., Lösschke, S., Möller, V., et al., Eds.; Cambridge University Press: Cambridge, UK; New York, NY, USA, 2022.
- Liu, J.; Hull, V.; Godfray, H.C.J.; Tilman, D.; Gleick, P.; Hoff, H.; Pahl-Wostl, C.; Xu, Z.; Chung, M.G.; Sun, J.; et al. Nexus Approaches to Global Sustainable Development. *Nat. Sustain.* **2018**, *1*, 466–476. [\[CrossRef\]](#)
- United Nations, Department of Economic and Social Affairs, Population Division. *World Urbanization Prospects: The 2018 Revision (ST/ESA/SER.A/420)*; United Nations: New York, NY, USA, 2019.
- Almenar, J.B.; Elliot, T.; Rugani, B.; Philippe, B.; Gutierrez, T.N.; Sonnemann, G.; Geneletti, D. Nexus between Nature-Based Solutions, Ecosystem Services and Urban Challenges. *Land Use Policy* **2021**, *100*, 104898. [\[CrossRef\]](#)
- Cortinovis, C.; Geneletti, D. A Framework to Explore the Effects of Urban Planning Decisions on Regulating Ecosystem Services in Cities. *Ecosyst. Serv.* **2019**, *38*, 100946. [\[CrossRef\]](#)
- Fang, C.; Yu, D. Urban Agglomeration: An Evolving Concept of an Emerging Phenomenon. *Landsc. Urban Plan.* **2017**, *162*, 126–136. [\[CrossRef\]](#)
- Li, L.; Ma, S.; Zheng, Y.; Xiao, X. Integrated Regional Development: Comparison of Urban Agglomeration Policies in China. *Land Use Policy* **2022**, *114*, 105939. [\[CrossRef\]](#)
- Yang, G.; Ge, Y.; Xue, H.; Yang, W.; Shi, Y.; Peng, C.; Du, Y.; Fan, X.; Ren, Y.; Chang, J. Using Ecosystem Service Bundles to Detect Trade-Offs and Synergies across Urban-Rural Complexes. *Landsc. Urban Plan.* **2015**, *136*, 110–121. [\[CrossRef\]](#)
- Fu, X.; Yao, L.; Xu, W.; Wang, Y.; Sun, S. Exploring the Multitemporal Surface Urban Heat Island Effect and Its Driving Relation in the Beijing-Tianjin-Hebei Urban Agglomeration. *Appl. Geogr.* **2022**, *144*, 102714. [\[CrossRef\]](#)
- Ouyang, X.; Wei, X.; Li, Y.; Wang, X.C.; Klemeš, J.J. Impacts of Urban Land Morphology on PM_{2.5} Concentration in the Urban Agglomerations of China. *J. Environ. Manag.* **2021**, *283*, 112000. [\[CrossRef\]](#)
- Wen, Y.; Zhang, Z.; Liang, D.; Xu, Z. Rural Residential Land Transition in the Beijing-Tianjin-Hebei Region: Spatial-Temporal Patterns and Policy Implications. *Land Use Policy* **2020**, *96*, 104700. [\[CrossRef\]](#)
- Zhang, D.; Huang, Q.; He, C.; Yin, D.; Liu, Z. Planning Urban Landscape to Maintain Key Ecosystem Services in a Rapidly Urbanizing Area: A Scenario Analysis in the Beijing-Tianjin-Hebei Urban Agglomeration, China. *Ecol. Indic.* **2019**, *96*, 559–571. [\[CrossRef\]](#)
- Sun, M.; Wang, J.; He, K. Analysis on the Urban Land Resources Carrying Capacity during Urbanization—A Case Study of Chinese YRD. *Appl. Geogr.* **2020**, *116*, 102170. [\[CrossRef\]](#)
- Feng, R.; Wang, F.; Wang, K.; Wang, H.; Li, L. Urban Ecological Land and Natural-Anthropogenic Environment Interactively Drive Surface Urban Heat Island: An Urban Agglomeration-Level Study in China. *Environ. Int.* **2021**, *157*, 106857. [\[CrossRef\]](#) [\[PubMed\]](#)
- Zhang, H.; Yin, Y.; An, H.; Lei, J.; Li, M.; Song, J.; Han, W. Surface Urban Heat Island and Its Relationship with Land Cover Change in Five Urban Agglomerations in China Based on GEE. *Environ. Sci. Pollut. Res.* **2022**, *29*, 82271–82285. [\[CrossRef\]](#)

16. Wang, Y.; Yao, L.; Xu, Y.; Sun, S.; Li, T. Potential Heterogeneity in the Relationship between Urbanization and Air Pollution, from the Perspective of Urban Agglomeration. *J. Clean. Prod.* **2021**, *298*, 126822. [CrossRef]
17. Zhao, R.; Zhan, L.; Yao, M.; Yang, L. A Geographically Weighted Regression Model Augmented by Geodetector Analysis and Principal Component Analysis for the Spatial Distribution of PM_{2.5}. *Sustain. Cities Soc.* **2020**, *56*, 102106. [CrossRef]
18. Mao, X.; Huang, X.; Song, Y.; Zhu, Y.; Tan, Q. Response to Urban Land Scarcity in Growing Megacities: Urban Containment or Inter-City Connection? *Cities* **2020**, *96*, 102399. [CrossRef]
19. Lafortezza, R.; Sanesi, G. Nature-Based Solutions: Settling the Issue of Sustainable Urbanization. *Environ. Res.* **2019**, *172*, 394–398. [CrossRef]
20. Tiftonell, P.; Struik, P.C.; Kuyper, T.W. Ecological Intensification of Agriculture—Sustainable by Nature. *Curr. Opin. Environ. Sustain.* **2014**, *8*, 53–61. [CrossRef]
21. Bush, J.; Doyon, A. Building Urban Resilience with Nature-Based Solutions: How Can Urban Planning Contribute? *Cities* **2019**, *95*, 102483. [CrossRef]
22. Nesshöver, C.; Assmuth, T.; Irvine, K.N.; Rusch, G.M.; Waylen, K.A.; Delbaere, B.; Haase, D.; Jones-Walters, L.; Keune, H.; Kovacs, E.; et al. The Science, Policy and Practice of Nature-Based Solutions: An Interdisciplinary Perspective. *Sci. Total Environ.* **2017**, *579*, 1215–1227. [CrossRef]
23. Westman, L.; Patterson, J.; Macrorie, R.; Orr, C.J.; Ashcraft, C.M.; Broto, V.C.; Dolan, D.; Gupta, M.; van der Heijden, J.; Hickmann, T.; et al. Compound Urban Crises. *Ambio* **2022**, *51*, 1402–1415. [CrossRef] [PubMed]
24. Cord, A.F.; Bartkowsky, B.; Beckmann, M.; Dittrich, A.; Hermans-Neumann, K.; Kaim, A.; Lienhoop, N.; Locher-Krause, K.; Priess, J.; Schröter-Schlaack, C.; et al. Towards Systematic Analyses of Ecosystem Service Trade-Offs and Synergies: Main Concepts, Methods and the Road Ahead. *Ecosyst. Serv.* **2017**, *28*, 264–272. [CrossRef]
25. Piracha, A.; Chaudhary, M.T. Urban Air Pollution, Urban Heat Island and Human Health: A Review of the Literature. *Sustainability* **2022**, *14*, 9234. [CrossRef]
26. Singh, N.; Singh, S.; Mall, R.K. Urban Ecology and Human Health: Implications of Urban Heat Island, Air Pollution and Climate Change Nexus. In *Urban Ecology*; Elsevier Inc.: Cambridge, MA, USA, 2020; pp. 317–334.
27. Niu, L.; Zhang, Z.; Peng, Z.; Liang, Y.; Liu, M.; Jiang, Y.; Wei, J.; Tang, R. Identifying Surface Urban Heat Island Drivers and Their Spatial Heterogeneity in China's 281 Cities: An Empirical Study Based on Multiscale Geographically Weighted Regression. *Remote Sens.* **2021**, *13*, 4428. [CrossRef]
28. Deilami, K.; Kamruzzaman, M.; Liu, Y. Urban Heat Island Effect: A Systematic Review of Spatio-Temporal Factors, Data, Methods, and Mitigation Measures. *Int. J. Appl. Earth Obs. Geoinf.* **2018**, *67*, 30–42. [CrossRef]
29. Guo, D. Local Entropy Map: A Nonparametric Approach to Detecting Spatially Varying Multivariate Relationships. *Int. J. Geogr. Inf. Sci.* **2010**, *24*, 1367–1389. [CrossRef]
30. Wang, J.F.; Li, X.H.; Christakos, G.; Liao, Y.L.; Zhang, T.; Gu, X.; Zheng, X.Y. Geographical Detectors-Based Health Risk Assessment and Its Application in the Neural Tube Defects Study of the Heshun Region, China. *Int. J. Geogr. Inf. Sci.* **2010**, *24*, 107–127. [CrossRef]
31. Wang, J.F.; Zhang, T.L.; Fu, B.J. A Measure of Spatial Stratified Heterogeneity. *Ecol. Indic.* **2016**, *67*, 250–256. [CrossRef]
32. Outline Development Plan for the Guangdong-Hong Kong-Macao Greater Bay Area. Available online: <https://www.bayarea.gov.hk/en/outline/plan.html> (accessed on 30 November 2022).
33. The Outline Plan of Beijing-Tianjin-Hebei Integrated Development. Available online: <http://jjj.chinadevelopment.com.cn/> (accessed on 30 November 2022). (In Chinese).
34. The Yangtze River Delta Integration Plan. Available online: http://www.gov.cn/zhengce/2019-12/01/content_5457442.htm (accessed on 30 November 2022). (In Chinese)
35. Wu, L.; Sun, C.; Fan, F. Estimating the Characteristic Spatiotemporal Variation in Habitat Quality Using the Invest Model—A Case Study from Guangdong–Hong Kong–Macao Greater Bay Area. *Remote Sens.* **2021**, *13*, 1008. [CrossRef]
36. Lin, M.; Lin, T.; Sun, C.; Jones, L.; Sui, J.; Zhao, Y.; Liu, J.; Xing, L.; Ye, H.; Zhang, G.; et al. Using the Eco-Erosion Index to Assess Regional Ecological Stress Due to Urbanization—A Case Study in the Yangtze River Delta Urban Agglomeration. *Ecol. Indic.* **2020**, *111*, 106028. [CrossRef]
37. Dong, L.; Longwu, L.; Zhenbo, W.; Liangkan, C.; Faming, Z. Exploration of Coupling Effects in the Economy–Society–Environment System in Urban Areas: Case Study of the Yangtze River Delta Urban Agglomeration. *Ecol. Indic.* **2021**, *128*, 107858. [CrossRef]
38. Wang, J.; Zhou, W.; Pickett, S.T.A.; Yu, W.; Li, W. A Multiscale Analysis of Urbanization Effects on Ecosystem Services Supply in an Urban Megaregion. *Sci. Total Environ.* **2019**, *662*, 824–833. [CrossRef] [PubMed]
39. Gao, K.; Yang, X.; Wang, Z.; Zhang, H.; Huang, C.; Zeng, X. Spatial Sustainable Development Assessment Using Fusing Multisource Data from the Perspective of Production-Living-Ecological Space Division: A Case of Greater Bay Area, China. *Remote Sens.* **2022**, *14*, 2772. [CrossRef]
40. Jiang, H.; Peng, J.; Dong, J.; Zhang, Z.; Xu, Z.; Meersmans, J. Linking Ecological Background and Demand to Identify Ecological Security Patterns across the Guangdong-Hong Kong-Macao Greater Bay Area in China. *Landsc. Ecol.* **2021**, *36*, 2135–2150. [CrossRef]
41. Lin, G.; Jiang, D.; Fu, J.; Cao, C.; Zhang, D. Spatial Conflict of Production-Living-Ecological Space and Sustainable-Development Scenario Simulation in Yangtze River Delta Agglomerations. *Sustainability* **2020**, *12*, 2175. [CrossRef]

42. Fang, G.; Wang, Q.; Tian, L. Green Development of Yangtze River Delta in China under Population-Resources-Environment-Development-Satisfaction Perspective. *Sci. Total Environ.* **2020**, *727*, 138710. [[CrossRef](#)] [[PubMed](#)]
43. Yang, Y.; Bao, W.; Liu, Y. Coupling Coordination Analysis of Rural Production-Living-Ecological Space in the Beijing-Tianjin-Hebei Region. *Ecol. Indic.* **2020**, *117*, 106512. [[CrossRef](#)]
44. Peng, C.; Li, B.; Nan, B. An Analysis Framework for the Ecological Security of Urban Agglomeration: A Case Study of the Beijing-Tianjin-Hebei Urban Agglomeration. *J. Clean. Prod.* **2021**, *315*, 128111. [[CrossRef](#)]
45. National Bureau of Statistics of China (NBSC). Available online: <http://www.stats.gov.cn/english/Statisticaldata/AnnualData/> (accessed on 30 November 2022).
46. Wang, X.; Yan, F.; Zeng, Y.; Chen, M.; Su, F.; Cui, Y. Changes in Ecosystems and Ecosystem Services in the Guangdong-Hong Kong-Macao Greater Bay Area since the Reform and Opening up in China. *Remote Sens.* **2021**, *13*, 1611. [[CrossRef](#)]
47. Zhou, M.; Lu, L.; Guo, H.; Weng, Q.; Cao, S.; Zhang, S.; Li, Q. Urban Sprawl and Changes in Land-Use Efficiency in the Beijing-Tianjin-Hebei Region, China from 2000 to 2020: A Spatiotemporal Analysis Using Earth Observation Data. *Remote Sens.* **2021**, *13*, 2850. [[CrossRef](#)]
48. Wu, J.; Li, X.; Luo, Y.; Zhang, D. Spatiotemporal Effects of Urban Sprawl on Habitat Quality in the Pearl River Delta from 1990 to 2018. *Sci. Rep.* **2021**, *11*, 1–15. [[CrossRef](#)] [[PubMed](#)]
49. Wang, H.; Tang, L.; Qiu, Q.; Chen, H. Assessing the Impacts of Urban Expansion on Habitat Quality by Combining the Concepts of Land Use, Landscape, and Habitat in Two Urban Agglomerations in China. *Sustainability* **2020**, *12*, 4346. [[CrossRef](#)]
50. He, C.; Gao, B.; Huang, Q.; Ma, Q.; Dou, Y. Environmental Degradation in the Urban Areas of China: Evidence from Multi-Source Remote Sensing Data. *Remote Sens. Environ.* **2017**, *193*, 65–75. [[CrossRef](#)]
51. Zhang, D.; Huang, Q.; He, C.; Wu, J. Impacts of Urban Expansion on Ecosystem Services in the Beijing-Tianjin-Hebei Urban Agglomeration, China: A Scenario Analysis Based on the Shared Socioeconomic Pathways. *Resour. Conserv. Recycl.* **2017**, *125*, 115–130. [[CrossRef](#)]
52. Lu, D.; Song, K.; Zang, S.; Jia, M.; Du, J.; Ren, C. The Effect of Urban Expansion on Urban Surface Temperature in Shenyang, China: An Analysis with Landsat Imagery. *Environ. Model. Assess.* **2015**, *20*, 197–210. [[CrossRef](#)]
53. Zhang, G.; Gao, Y.; Li, J.; Su, B.; Chen, Z.; Lin, W. China's Environmental Policy Intensity for 1978–2019. *Sci. Data* **2022**, *9*, 75. [[CrossRef](#)]
54. European Space Agency (ESA). Land Cover CCI Product User Guide Version Tech Rep. 2017. Available online: http://maps.elie.ucl.ac.be/CCI/viewer/download/ESACCI-LC-Ph2-PUGv2_2.0.pdf (accessed on 30 November 2022).
55. IUCN Habitats Classification Scheme. Available online: <https://www.iucnredlist.org/resources/habitat-classification-scheme> (accessed on 30 November 2022).
56. Jung, M.; Dahal, P.R.; Butchart, S.H.M.; Donald, P.F.; De Lamo, X.; Lesiv, M.; Kapos, V.; Rondinini, C.; Visconti, P. A Global Map of Terrestrial Habitat Types. *Sci. Data* **2020**, *7*, 1–8. [[CrossRef](#)]
57. Wei, J.; Li, Z.; Cribb, M.; Huang, W.; Xue, W.; Sun, L.; Guo, J.; Peng, Y.; Li, J.; Lyapustin, A.; et al. Improved 1km Resolution PM2.5 Estimates across China Using Enhanced Space-Time Extremely Randomized Trees. *Atmos. Chem. Phys.* **2020**, *20*, 3273–3289. [[CrossRef](#)]
58. Wei, J.; Li, Z.; Lyapustin, A.; Sun, L.; Peng, Y.; Xue, W.; Su, T.; Cribb, M. Reconstructing 1-Km-Resolution High-Quality PM2.5 Data Records from 2000 to 2018 in China: Spatiotemporal Variations and Policy Implications. *Remote Sens. Environ.* **2021**, *252*, 112136. [[CrossRef](#)]
59. Lloyd, C.T.; Sorichetta, A.; Tatem, A.J. High Resolution Global Gridded Data for Use in Population Studies. *Sci. Data* **2017**, *4*, 170001. [[CrossRef](#)]
60. Natural Capital Project. InVEST-Habitat Quality. Available online: https://storage.googleapis.com/releases.naturalcapitalproject.org/invest-userguide/latest/habitat_quality.html (accessed on 30 November 2022).
61. Hall, L.S.; Krausman, P.R.; Morrison, M.L. The Habitat Concept and a Plea for Standard Terminology Key Words Peer Refereed. *Wildl. Soc. Bull.* **1997**, *25*, 173–182.
62. McKinney, M.L. Urbanization, Biodiversity, and Conservation. *Bioscience* **2002**, *52*, 883–890. [[CrossRef](#)]
63. Tang, F.; Fu, M.; Wang, L.; Song, W.; Yu, J.; Wu, Y. Dynamic Evolution and Scenario Simulation of Habitat Quality under the Impact of Land-Use Change in the Huaihe River Economic Belt, China. *PLoS ONE* **2021**, *16*, e0249566. [[CrossRef](#)] [[PubMed](#)]
64. Chen, T.; Feng, Z.; Zhao, H.; Wu, K. Dataset of Ecosystem Services in Beijing and Its Surrounding Areas. *Data Br.* **2020**, *29*, 105151. [[CrossRef](#)] [[PubMed](#)]
65. Xu, L.; Chen, S.S.; Xu, Y.; Li, G.; Su, W. Impacts of Land-Use Change on Habitat Quality during 1985–2015 in the Taihu Lake Basin. *Sustainability* **2019**, *11*, 3513. [[CrossRef](#)]
66. Li, F.; Wang, L.; Chen, Z.; Clarke, K.C.; Li, M.; Jiang, P. Extending the SLEUTH Model to Integrate Habitat Quality into Urban Growth Simulation. *J. Environ. Manag.* **2018**, *217*, 486–498. [[CrossRef](#)]
67. Zhou, D.; Xiao, J.; Bonafoni, S.; Berger, C.; Deilami, K.; Zhou, Y.; Froelking, S.; Yao, R.; Qiao, Z.; Sobrino, J.A. Satellite Remote Sensing of Surface Urban Heat Islands: Progress, Challenges, and Perspectives. *Remote Sens.* **2019**, *11*, 48. [[CrossRef](#)]
68. Liu, F.; Zhang, X.; Murayama, Y.; Morimoto, T. Impacts of Land Cover/Use on the Urban Thermal Environment: A Comparative Study of 10 Megacities in China. *Remote Sens.* **2020**, *12*, 307. [[CrossRef](#)]

69. Wang, Q.; Wang, H.; Zeng, H.; Chang, R.; Bai, X. Understanding Relationships between Landscape Multifunctionality and Land-Use Change across Spatiotemporal Characteristics: Implications for Supporting Landscape Management Decisions. *J. Clean. Prod.* **2022**, *377*, 134474. [[CrossRef](#)]
70. Naimi, B.; Hamm, N.A.S.; Groen, T.A.; Skidmore, A.K.; Toxopeus, A.G.; Alibakhshi, S. ELSA: Entropy-Based Local Indicator of Spatial Association. *Spat. Stat.* **2019**, *29*, 66–88. [[CrossRef](#)]
71. Kalantari, M.; Ghavagh, A.R.; Toomanian, A.; Dero, Q.Y. A New Methodological Framework for Crime Spatial Analysis Using Local Entropy Map. *Mod. Appl. Sci.* **2016**, *10*, 179. [[CrossRef](#)]
72. Yaakub, N.F.; Masron, T.; Marzuki, A.; Soda, R. GIS-Based Spatial Correlation Analysis: Sustainable Development and Two Generations of Demographic Changes. *Sustainability* **2022**, *14*, 1490. [[CrossRef](#)]
73. Wang, H.; Qin, F.; Xu, C.; Li, B.; Guo, L.; Wang, Z. Evaluating the Suitability of Urban Development Land with a Geodetector. *Ecol. Indic.* **2021**, *123*, 107339. [[CrossRef](#)]
74. Zhang, X.; Liao, L.; Xu, Z.; Zhang, J.; Chi, M.; Lan, S.; Gan, Q. Interactive Effects on Habitat Quality Using InVEST and GeoDetector Models in Wenzhou, China. *Land* **2022**, *11*, 630. [[CrossRef](#)]
75. Wang, Y.; Guo, Z.; Han, J. The Relationship between Urban Heat Island and Air Pollutants and Them with Influencing Factors in the Yangtze River Delta, China. *Ecol. Indic.* **2021**, *129*, 107976. [[CrossRef](#)]
76. Yang, Y.; Zheng, Z.; Yim, S.Y.L.; Roth, M.; Ren, G.; Gao, Z.; Wang, T.; Li, Q.; Shi, C.; Ning, G.; et al. PM2.5 Pollution Modulates Wintertime Urban Heat Island Intensity in the Beijing-Tianjin-Hebei Megalopolis, China. *Geophys. Res. Lett.* **2020**, *47*, e2019GL084288. [[CrossRef](#)]
77. Wu, H.; Wang, T.; Wang, Q.; Riemer, N.; Cao, Y.; Liu, C.; Ma, C.; Xie, X. Relieved Air Pollution Enhanced Urban Heat Island Intensity in the Yangtze River Delta, China. *Aerosol Air Qual. Res.* **2019**, *19*, 2683–2696. [[CrossRef](#)]
78. Wu, D.; Xu, Y.; Zhang, S. Will Joint Regional Air Pollution Control Be More Cost-Effective? An Empirical Study of China's Beijing-Tianjin-Hebei Region. *J. Environ. Manag.* **2015**, *149*, 27–36.
79. Wang, L.; Zhang, F.; Pilot, E.; Yu, J.; Nie, C.; Holdaway, J.; Yang, L.; Li, Y.; Wang, W.; Vardoulakis, S.; et al. Taking Action on Air Pollution Control in the Beijing-Tianjin-Hebei (BTH) Region: Progress, Challenges and Opportunities. *Int. J. Environ. Res. Public Health* **2018**, *15*, 306. [[CrossRef](#)]
80. Li, Y.; Huang, S.; Yin, C.; Sun, G.; Ge, C. Construction and Countermeasure Discussion on Government Performance Evaluation Model of Air Pollution Control: A Case Study from Beijing-Tianjin-Hebei Region. *J. Clean. Prod.* **2020**, *254*, 120072. [[CrossRef](#)]
81. Li, Y.; Zhang, L.; Qiu, J.; Yan, J.; Wan, L.; Wang, P.; Hu, N.; Cheng, W.; Fu, B. Spatially Explicit Quantification of the Interactions among Ecosystem Services. *Landsc. Ecol.* **2017**, *32*, 1181–1199. [[CrossRef](#)]
82. Shen, J.; Li, S.; Liang, Z.; Liu, L.; Li, D.; Wu, S. Exploring the Heterogeneity and Nonlinearity of Trade-Offs and Synergies among Ecosystem Services Bundles in the Beijing-Tianjin-Hebei Urban Agglomeration. *Ecosyst. Serv.* **2020**, *43*, 101103. [[CrossRef](#)]
83. Li, G.; Fang, C.; Wang, S. Exploring Spatiotemporal Changes in Ecosystem-Service Values and Hotspots in China. *Sci. Total Environ.* **2016**, *545–546*, 609–620. [[CrossRef](#)] [[PubMed](#)]
84. Hou, Y.; Li, B.; Müller, F.; Fu, Q.; Chen, W. A Conservation Decision-Making Framework Based on Ecosystem Service Hotspot and Interaction Analyses on Multiple Scales. *Sci. Total Environ.* **2018**, *643*, 277–291. [[CrossRef](#)] [[PubMed](#)]

Disclaimer/Publisher's Note: The statements, opinions and data contained in all publications are solely those of the individual author(s) and contributor(s) and not of MDPI and/or the editor(s). MDPI and/or the editor(s) disclaim responsibility for any injury to people or property resulting from any ideas, methods, instructions or products referred to in the content.